Earth-Science Reviews 231 (2022) 104094

Contents lists available at ScienceDirect

Earth-Science Reviews

journal homepage: www.elsevier.com/locate/earscirev

Structure of the south-central Taiwan fold-and-thrust belt: Testing the viability of the model

D. Brown [a,*], J. Alvarez-Marron [a], G. Camanni [b], C. Biete [c], H. Kuo-Chen [d], Y.-M. Wu [d,e]

[a] Geosciences Barcelona, CSIC, 08028 Barcelona, Spain
[b] DiSTAR, Università degli Studi di Napoli "Federico II", Naples, Italy
[c] c/Espronceda, 08005 Barcelona, Spain
[d] Department of Geosciences, National Taiwan University, 10617 Taipei, Taiwan
[e] Institute of Earth Sciences, Academia Sinica, Taipei 11529, Taiwan

ARTICLE INFO

Keywords:
Taiwan
Fold-and-thrust belt
Crystalline basement
Imbricate thrust system
Shortening
Fault reactivation
Seismicity
GPS
Topography

ABSTRACT

A structural model is developed for the south-central Taiwan fold-and-thrust belt that shows consistency across an array of data types and marks an important step forward in the consideration of geological hazards and risks. Although there is general agreement about the regional scale geology of Taiwan, there are considerable differences in the structural interpretations of its western fold-and-thrust belt. In this paper, we bring together results of our previous studies and add new data and data analyses to develop a consistent 3D structural model for the south-central Taiwan fold-and-thrust belt that can explain key aspects of the seismicity, GPS, and topography data. We interpret the fold-and-thrust belt to be a west-verging, imbricate thrust system developed above a single basal thrust that is breached by ENE-striking faults that are inherited from the continental margin. These breaching faults are associated with ENE-striking transverse zones in the fold-and-thrust belt that are marked by changes in stratigraphy, structural style, strike and dip of the basal thrust, and uplift of the stratigraphic contacts. Along the eastern flank of the fold-and-thrust belt, metamorphic basement rocks are involved in the thrusting. Shortening estimates range from 15 km to >25 km. Much of the seismicity is taking place beneath the basal thrust, in the basement, along the flanks of basement highs and lows where strike-slip and transpressive fault types are common. There are systematic changes in GPS displacement vectors and strain rates across the transverse zones. Topography is higher in areas where basement is involved in the thrusting. The proposed structural model has depth and along-strike consistency, and can explain aspects of the distribution of seismicity, faults types, GPS displacement vectors and strain rates, and topography of the study area, and can therefore be considered a viable model.

1. Introduction

Understanding the structure and evolution of the Taiwan fold-and-thrust belt is an important and on-going research objective that has made it an example for the development of ideas about fault-related folding (e.g., kink-band folding, fault-bend folding (Suppe and Namson, 1979; Suppe and Chang, 1983), fold-and-thrust belt architecture and evolution (e.g., Suppe, 1980, 1981; Namson, 1981; Carena et al., 2002; Mouthereau et al., 2001, 2002; Yue et al., 2005; Yang et al., 2007, 2016; Malavieille and Trullenque, 2009; Rodriguez-Roa and Wiltschko, 2010; Alvarez-Marron et al., 2014; Brown et al., 2017), and mechanics (i.e., the critical wedge model of Davis et al. (1983) and Dahlen et al. (1984)). While there is general agreement about the regional scale geology of the Taiwan fold-and-thrust belt there are, nevertheless, considerable differences in the structural interpretations about the location of the basal thrust, whether there is crystalline basement involved in the thrusting, if there is triangle zone, or duplex (including antiformal stack) development at the front, the existence, location and orientation of transfer zones, and the amount of shortening that is being accomodated. Because the Taiwan fold-and-thrust belt is currently active, having a structural model for it that has along-strike consistency across an array of data types is of considerable social importance since it has a significant impact on how geological hazards and risks are viewed and modelled (e.g., Loh et al., 1991; Campbell et al., 2002; Cheng et al., 2007; Camanni et al., 2014a; Wu et al., 2017).

Since 2006, our research group has carried out extensive new field

* Corresponding author.
E-mail address: dbrown@geo3bcn.csic.es (D. Brown).

https://doi.org/10.1016/j.earscirev.2022.104094
Received 25 April 2022; Received in revised form 10 June 2022; Accepted 16 June 2022
Available online 20 June 2022

mapping in south-central Taiwan (Fig. 1). The aim has been to investigate the structure of the fold-and-thrust belt and the influence of inherited structures that were located on the continental margin that is entering into the deformation (e.g., Brown et al., 2012, 2017; Alvarez-Marron et al., 2014; Camanni et al., 2014a, 2014b, 2016; Biete et al., 2018, 2019). In this paper we bring together these studies, first presenting a proxy for the crystalline basement-to-cover interface derived from a P-wave tomographic model (Kuo-Chen et al., 2012) that we then integrate with our field mapping to construct a structural model that has 3D consistency. As a proof of concept, we then test whether or not this model can explain aspects of the seismicity, GPS, and topography data from the south-central part of the Taiwan fold-and-thrust belt.

2. Geological background

2.1. The southeast margin of the Eurasian plate

Taiwan (Fig. 1A) is an active mountain belt that has been forming since the Late Miocene as the result of the collision of the Luzon arc with the deeply subducting Eurasian margin (e.g., Teng, 1990; Sibuet and Hsu, 1997; Sibuet and Hsu, 2004, Huang et al., 2014a). To better understand the structure of the Taiwan fold-and-thrust belt it is important to have a first-order understanding of the morphology, geology, structure, and Mesozoic through Holocene evolution of the part of the Eurasian margin that is now entering into the deformation taking place in western Taiwan (e.g., Camanni and Ye, 2022). The morphology of the margin to the west of Taiwan consists of a broad proximal zone, a roughly northeast-striking slope break (roughly the 200-m bathymetry contour), a slope, and a broad distal zone (Fig. 1). The structure of the margin is comprised of a shelf area with fault-bound, Eocene-age basins, a necking zone where the basement thins from the shelf to the distal margin (e.g., Mohn et al., 2012), and a c. 300 km wide hyper-extended margin (Fig. 1). The crustal thickness of the shelf is 30 +/− 5 km (Yeh et al., 1998; Kim et al., 2005; Kuo-Chen et al., 2012; Huang et al., 2014a, 2014b; Wu et al., 2014; Chen et al., 2016), thinning to approximately 18 km along the hyper-extended part of the margin (Fig. 1B) (Chen and Yang, 1996; Li et al., 2007; Lin et al., 2008; Huang et al., 2012; Yeh et al., 2012; Deng et al., 2012; McIntosh et al., 2013, 2014). The transition from the margin's continental crust to the oceanic crust of the South China Sea occurs to the south of the area shown in Fig. 1 (e.g., Nissen et al., 1995; Zhao et al., 2010; Tsai et al., 2004: Deng et al., 2012; Yeh et al., 2012; McIntosh et al., 2013; Lester et al., 2014). Importantly for this paper, the structural and geomorphological grain of the margin that is entering into the deformation is roughly ENE-WSW, which is at a high angle to the approximately N-S structural grain of the fold-and-thrust belt (Fig. 1).

The Mesozoic pre-rift geology and lithostratigraphy of the shelf area that is entering into the Taiwan mountain belt is not well known, although the depth to the top of the Mesozoic has been mapped in some detail (Fig. 1) (Lin et al., 2003). Eocene-age synrift basins are oriented roughly northeast-southwest (Hsu, 2001; Lin and Watts, 2002; Lin et al., 2003; Teng and Lin, 2004; Lin et al., 2005; Cukur et al., 2011), and they locally accumulated up to c. 5 km of sediments (e.g., Lin et al., 2003). The Taihsi Basin, and in particular its eastern flank, the Hsuehshan Trough (Range in Fig. 1A) (Teng et al., 1991; Teng and Lin, 2004), is being deformed in central and northwestern Taiwan (Fig. 1a). The late Miocene extensional basins on the outer shelf and necking zone of the margin (of interest to this paper is the Tainan Basin) have roughly east-northeast striking bounding faults (Yang et al., 1991, 2016; Lee et al., 1993; Lin et al., 2003; Lin et al., 2005; Ding et al., 2008; Shi et al., 2008; Tang and Zheng, 2010).

2.2. Geological provinces of the Taiwan Orogen

The Taiwan orogen is divided into five roughly N-S oriented geological provinces that are separated by major faults (Fig. 1A). From west to east these zones are: the Coastal Plain, the Western Foothills, the Hsuehshan Range, the Central Range, and the Coastal Range. In much of south-central Taiwan, the boundary between the Coastal Plain and the Western Foothills is interpreted to coincide with the mostly buried tip line of the Changhua thrust (ChT in Fig. 1A). In the north of the study area, the Western Foothills is juxtaposed against the Hsuehshan Range across the Shuilikeng Fault (SkF). In the east, the Hsuehshan Range is juxtaposed against the Central Range across the Lishan Fault (LF). Southward, the Shuilikeng and Lishan faults link up with one another and the Central Range is juxtaposed against the Western Foothills along the Chaochou Fault (ChF). In what follows, we interpret the Coastal Plain, the Western Foothills, and the Hsuehshan Range to make up the fold-and-thrust belt in south-central Taiwan. The Central Range makes up the internal part of the orogeny as it is comprised of weakly metamorphosed Cenozoic clastic sediments with Mesozoic crystalline rocks forming the basement on which they were deposited.

2.3. Stratigraphy of the south-central Taiwan fold-and-thrust belt

The Mesozoic basement rocks do not crop out in the fold-and-thrust belt. However, in the Central Range where they do crop out they are comprised predominantly of marble and schist (Stanley et al., 1981; Ernst, 1983; Ho, 1988; Lan et al., 2008). The absolute ages of these rocks are not well constrained, although a number of Permian to Cretaceous isotopic ages have been determined (Jahn et al., 1986; Lo and Onstott, 1995; Lan et al., 2008; Yui et al., 2009, 2012; Wintsch et al., 2011). In western Taiwan and its offshore, several boreholes have intersected weakly metamorphosed siliciclastic and carbonate rocks that have been interpreted to range in age from Late Permian to Cretaceous (e.g., Jahn et al., 1992; Chiu, 1975; Ho, 1988; Shaw, 1996), although there is disagreement about the interpretations of the age of these rocks (e.g., Chiu, 1975; Ho, 1988; Shaw, 1996).

While the rocks of the Hsuehshan Range are accepted to be Eocene and Oligocene in age (e.g., Ho, 1988; Chen et al., 2009; Huang et al., 2012, 2013) (Fig. 1A), in the study area the paucity of age-determinant fossils complicates the understanding of the Eocene-aged stratigraphy. Furthermore, the rocks of the Hsuehshan Range are faulted and folded and, along its eastern and southern flank, a penetrative slaty cleavage is ubiquitous in the fine-grained units (e.g., Brown et al., 2012), making any estimate of thickness approximate. The lowest Eocene stratigraphic unit that crops out is the Chiayang Fm, which is comprised of up to 2000 m of thick-bedded sandstone and shale. The Chiayang Fm is overlain by the Shipachungshi Fm, an up to 1000-m-thick unit of thin-bedded sandstone and mudstone. The Shipachungschi Fm is conformably overlain by the Paileng Fm. The Paileng Fm consists of 4000 to 5000 m of thick-bedded, coarse-grained sandstone with quartz-pebble conglomerate and argillite at its base (the Tachien member), overlain by interbedded sandstone and bioturbated argillite and, at the top, coarse-grained to quartz-pebble conglomerate with minor amounts of lithofragments and feldspar. The Tachien member has been dated by large foraminifera to be late early to middle Eocene in age (Chen et al., 2009). Locally, in the northern part of the study area, middle to late Eocene-age (Huang et al., 2013) volcanic rocks of the Tsukeng Fm overlie the Paileng Fm (Chiu, 1975). Regionally, the Paileng Fm is unconformably overlain by several hundred meters of early Oligocene sandstone and shale of the Shuichangliu Fm (Fig. 2). This unconformity is interpreted to be the break-up unconformity that preceded the opening of the South China Sea (e.g., Teng, 1992; Lin et al., 2003; Huang et al., 2017).

In this paper, the chronostratigraphic nomenclature scheme of Alvarez-Marron et al. (2014) and Brown et al. (2017) is used for the Miocene and younger rocks (Fig. 2). This scheme follows the north to south stratigraphic correlation of Shea et al. (2003). In south-central Taiwan, the outcropping Miocene rocks can be broadly divided into four formations. The early Miocene Takeng Fm is comprised of approximately 800 to 1000 m of thick-bedded sandstone at the base,

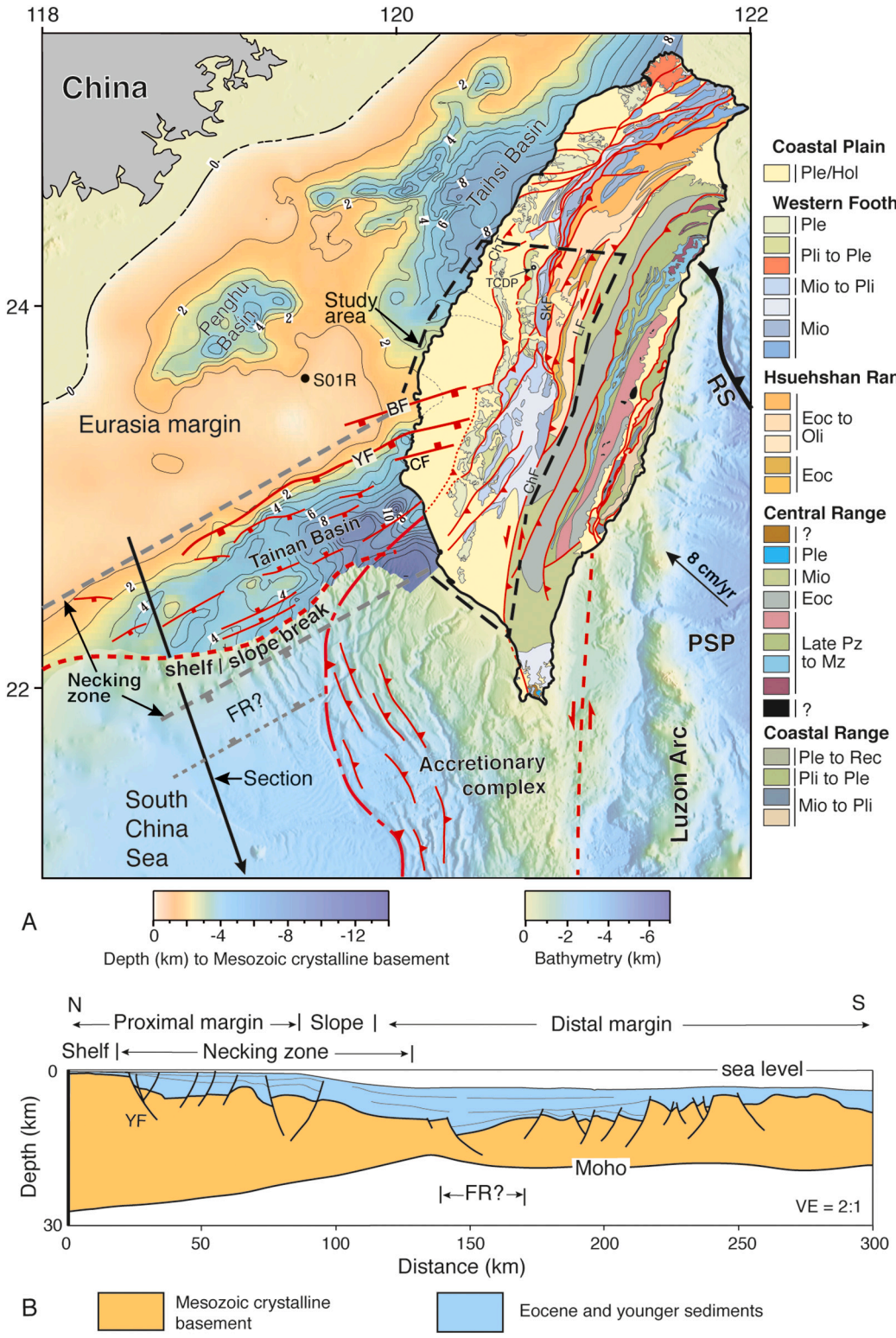

Fig. 1. A) Geological map of Taiwan (redrawn from Chen, 2000). The depth to the top of the Mesozoic basement in the Taiwan Strait is from Lin et al. (2003). The location of the necking zone is indicated by the dashed gray lines, and the shelf-slope break by the dashed red line. Bathymetry is shown to the south and east of Taiwan. The location of the study area is shown, as is the location of GPS station S01R and Taiwan Chelungpu Fault Drilling Project borehole A (TCDP). RS = Ryukyu subduction zone, PSP = Philipinne Sea Plate, ChT = Changhua Thrust, SkF = Shuilikeng Fault, LF = Lishan Fault, ChF = Chaochou Fault, BF = B fault, YF = Yichu fault, CF = C fault. B) A schematic cross section of the continental margin to the southwest of Taiwan showing the terminology used in the text. The location of the section is shown in Fig. 1A. The structure of the slope and distal margin is simplified from Yeh et al. (2012) and Lester et al. (2014). The continent to ocean transition lies to the south of this diagram. FR = failed rift of Yeh et al. (2012), Lester et al. (2014), and McIntosh et al. (2014). YF = Yichu fault. The vertical exaggeration is 2:1. (For interpretation of the references to colour in this figure legend, the reader is referred to the web version of this article.)

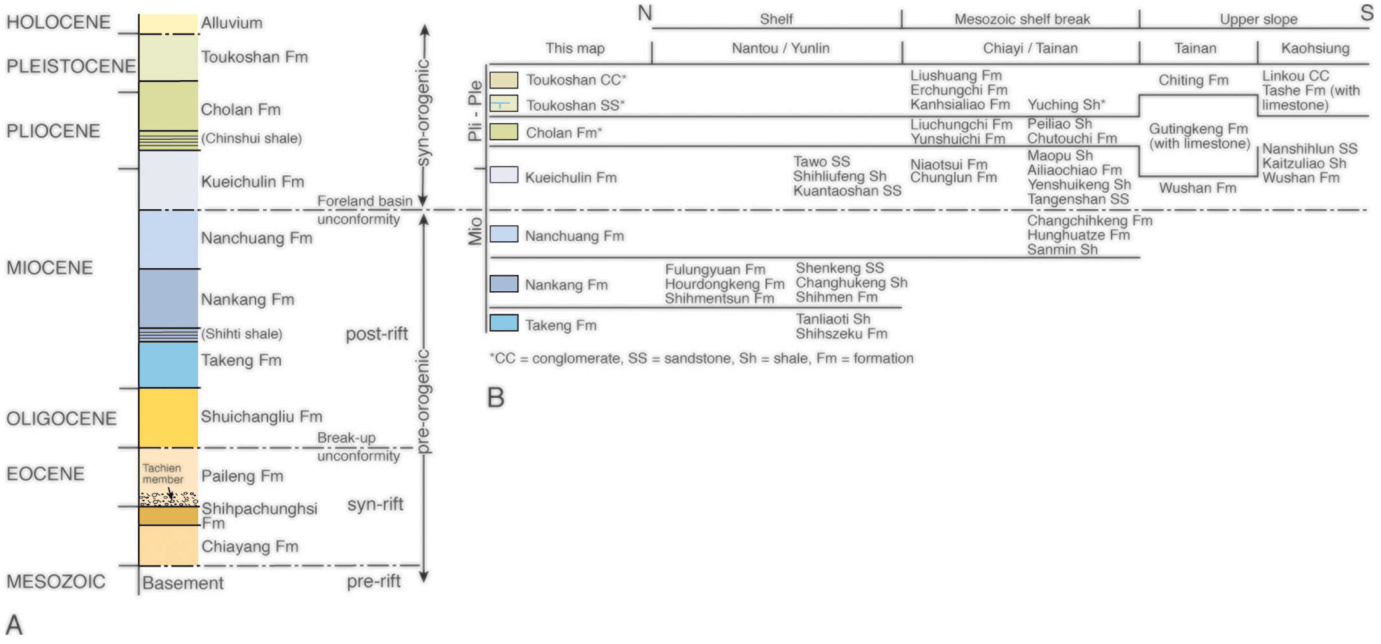

Fig. 2. A) General stratigraphy and tectonostratigraphic units showing the names of formations used in this study. B) A chronostratigraphic chart that shows the correlations used in the mapping. The correlation is based on that of Shea et al. (2003).

overlain by thin-bedded sandstone and shale near the top. The Takeng Fm is overlain by up to 500 m of shale (Shihti shale at the base) and thick-bedded sandstone of the Nankang Fm. The Nankang Fm is in turn overlain by the Nanchuang Fm. Although, locally, in the northernmost part of the study area, the Nankang Fm is unconformably overlain by the Kueichulin Fm. The Nanchuang Fm is made up of thin- to thick-bedded sandstone intercalated with shale. Its thickness varies widely across the study area, ranging from several hundred meters in the north to >2000 m in the south. It is unconformably overlain by the latest Miocene to early Pliocene Kueichulin Fm, which is comprised of 150 m to >3000 m of thin- to very thick-bedded muddy sandstone and sandy mudstone. The Kueichulin Fm is conformably overlain by the Pliocene- to Pleistocene-aged Cholan Fm. The base of the Cholan Fm is comprised of the several hundred-meter-thick Chinshui shale unit, followed upward by up to 3000 m of interbedded mudstone, shale, and sandstone. The Cholan Fm is conformably overlain by the Pleistocene Toukoshan Fm, a coarsening upward sequence made up of thick-bedded sandstone with shale interbeds that, upward, becomes interfingered with, and eventually completely replaced by conglomerate. In parts of the map area, the Toukoshan Fm may reach a thickness of up to 5000 m and, in the south, it has a number of unconformities. It is overlain by Holocene-age gravels that, in places, are several hundred meters thick.

In tectonostratigraphic terms for the Taiwan orogen, the Mesozoic rocks form the pre-rift, the Eocene the *syn*-rift, the Oligocene to late Miocene the post-rift, and the late Miocene through Holocene is the syn-orogenic (Fig. 2A). In this paper, we define the pre-rift Mesozoic rocks as the crystalline basement and assume that it is comprised of similar lithologies as the Mesozoic rocks found in the Central Range. Because of its regionally developed unconformity (Lin and Watts, 2002; Tensi et al., 2006), the base of the late Miocene-age Kueichulin Fm is taken to mark the onset of sedimentation in the foreland basin. This is in contrast to Teng (1987), Covey (1986), and Hong (1997), who suggest that the onset of foreland basin sedimentation occurred during the early Pliocene, and is recorded by the first appearance of slate clasts in the Chinshui shale at the base of the Cholan Fm.

3. Data description and methodologies

3.1. *P-wave velocity and a proxy for the basement-cover interface*

The involvement of crystalline basement in the deformation in a fold-and-thrust belt has implications for the geometric construction of cross sections, for the amount of shortening, the location of the basal thrust, or the transition into the metamorphic internal part of the mountain belt, among other things (e.g., Hatcher and Williams, 1986; Pfiffner, 2017; Poblet and Lisle, 2011; Lacombe and Bellahsen, 2016; Tavani et al., 2021). Therefore, in the interpretation of the structure that follows, it is important to have an estimate of the depth to the basement-cover interface. Since crystalline basement does not crop out in the south-central Taiwan fold-and-thrust belt, we use a petrophysical approach to define a proxy for the basement-cover interface that we can then use to interpret where (and if) basement is involved in the thrusting. We choose a P-wave velocity (Vp) of 5.2 km/s as a proxy for the basement-cover interface for the following reasons; 1) it is in keeping with the upper range of Vp determined from laboratory measurements carried out on clastic rocks and at the lower range of common crustal crystalline rocks (Fig. 3) (Christensen, 1989; Johnston and Christensen, 1992, 1993; Mavko et al., 2009; Christensen and Stanley, 2003; Brocher, 2005) and, 2) it is in keeping with the measured Vp (<5 km/s) of the late Miocene and younger sediments intersected by the Taiwan Chelungpu Fault Drilling Project borehole A (Wang et al., 2009).

3.1.1. *Vp data, methodology and uncertainties*

The depth and geometry of the Vp 5.2 km/s isovelocity surface is derived from the TAIGER local Vp model of Kuo-Chen et al. (2012). In this velocity model, the upper 24 km of the crust, which is the part of interest here, the discretization of the 3D velocity grid is 4 × 4 km horizontally and 2 km vertically, and at these depths we can expect a resolution of at least 20 × 20 km in the horizontal and 10 km vertical. We refer the reader to Kuo-Chen et al. (2012) for a detailed description of the acquisition and processing parameters, as well as the resolution testing, of the TAIGER data set.

The 5.2 km/s isovelocity surface is, however, a proxy and is meant to help with the interpretation of the approximate location and shape of basement-cover interface. A key uncertainty in the use of the 5.2 km/s

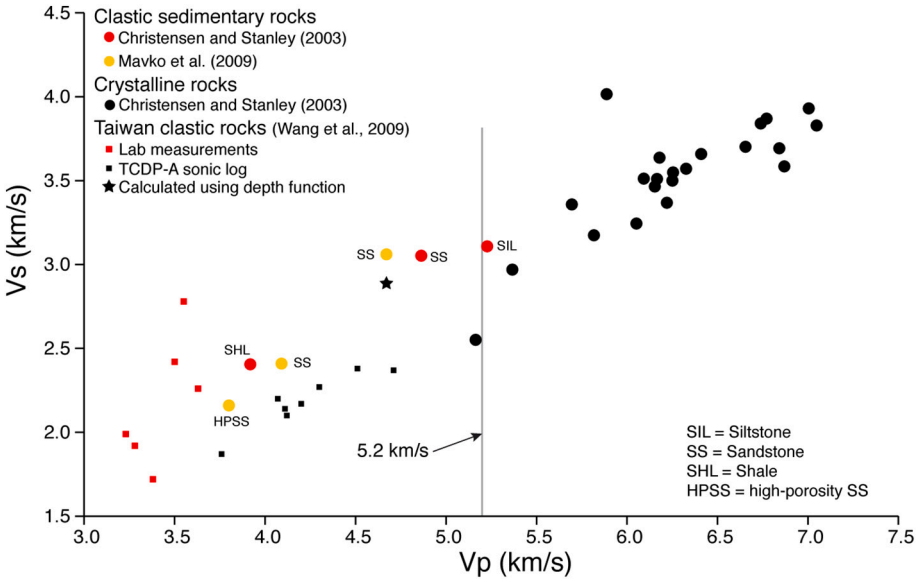

Fig. 3. Plot of P-wave (Vp) versus S-wave (Vs) normalised to 120 MPa (c. 5 km depth) and 125 °C for various crystalline rocks (Christensen and Stanley, 2003) and clastic sedimentary rocks (Mavko et al., 2009). Also shown are lab and sonic log measurements of Vp and Vs made on clastic sedimentary rocks (Wang et al., 2009) from different depths in the Taiwan Chelungpu Fault Drilling Project borehole A (TCDP) borehole (Fig. 1). The star indicates the calculated Vp and Vs of TCDP borehole rocks using the velocity to depth functions of Wang et al. (2009). A Vp of 5.2 km/s separates crystalline from clastic sedimentary rocks and is our proxy for the crystalline basement-cover interface in the south-central Taiwan fold-and-thrust belt.

isovelocity surface as a proxy for the basement-cover interface is that the lithology of the basement rocks in south-central Taiwan is not well known. A further uncertainty, especially in the depth and shape, is the resolution of the velocity model. These uncertainties mean that the 5.2 km/s proxy for the basement-cover interface may not be valid in detail everywhere. Nevertheless, the major features described below are also found in the Vp tomography models of Kim et al. (2005), Wu et al. (2007), and Huang et al. (2014b), so we think they are robust features that can be reliably interpreted.

3.1.2. *Vp and a proxy for the basement-cover interface*

Throughout the study area, at 4 km depth Vp is everywhere <5.2 km/s except along the central, eastern part of the Western Foothills (WF) and in the Hsuehshan Range (HR) (Fig. 4A). To the north of c. 24°, the Coastal Plain (CP) and Western Foothills (WF) areas are characterized by Vp >5.2 km/s at 6 km depth (with two small areas of lower Vp) and, at 8 km depth, Vp is almost everywhere >5.4 km/s (Fig. 4B and C). The Hsuehshan Range (HR) is almost everywhere characterized by Vp >5.2 km/s with, locally, Vp >5.8 km/s along the Lishan fault (LF). To the south of c. 24°, the Coastal Plain and the Western Foothills is characterized by Vp <5 km/s at 4 km depth, with the exception of an area of Vp >5.2 km/s to the west of the southern part of the Shuilikeng fault (SkF). At 6 km depth, much of the area to the south of 24° has Vp >5.2 km/s and, at 8 km depth, Vp is almost everywhere >5.4 km/s.

On the basis of our proposal that the 5.2 km/s isovelocity surface be used as a proxy for the basement-cover interface, a number of basement highs and lows can be interpreted beneath the Coastal Plain and the Western Foothills. Among these, the Tainan (TBH), Peikang (PBH), Alishan (ABH), and Northern (NBH) highs reach <5 km below sea level (Fig. 4D). The nearly continuous Hsuehshan basement high (HBH) reaches as shallow as 0 km below sea level, locally. Both the Central (CBL) and the Pingtung (PBL) basement lows reach >8 km depth.

3.2. *Structure of the south-central Taiwan fold-and-thrust belt*

3.2.1. *Data, methodology and uncertainties*

The structural analyses and interpretations that follow are based on new geological mapping (Fig. 5) carried out over 11 field campaigns during which >6000 structural and lithological observations were made at around 3000 data points over an area of approximately 13,000 km^2. The mapping was carried out at 1:50,000 and 1:25,000 scales using the geological maps of the Central Geological Survey of Taiwan as a base. The final map was drawn at 1:100,000 scale (Supplementary data set 1) using the chronostratigraphic scheme presented in Fig. 2. For reasons of clarity, in Fig. 5 only representative structural data are shown. In the map, the major thrusts and their names have been correlated from north to south (see Ho (1988) for a similar correlation).

Thirteen cross sections (Fig. 6) were constructed using the geological map, field structural data, published borehole information, and standard section construction techniques (Dahlstrom, 1969; Hossack, 1979; De Paor, 1988). All cross sections are oriented perpendicular to the regional strike of structures (bedding, thrusts, and major fold axial traces). Borehole lithological information was projected along the bedding strike onto the plane of the section. Where possible, the cross sections were restored by conserving bed-length (while conserving area) until they were deemed to be viable (Supplementary data 2). These sections can, therefore, be considered as balanced. Because of the absence of stratigraphic cutoffs, out-of-sequence thrusting, and a penetrative cleavage in the Hsuehshan Range, sections 1, 2 and 3 could not be restored. For balancing the cross sections, the western pin line was placed in the undeformed rocks to the west of the tip line of the frontal thrust and the sections were restored to a horizontal top of the Kueichulin Fm, a regional-scale marker that can be mapped throughout much of the study area. For restoration, a forward propagation (piggy-back) sequence of thrusting was assumed. Minimum shortening (length difference between the deformed and undeformed section) and fault displacement (distance a cut-off moved along a fault surface) estimates were made for the restored sections (Table 1). In an iterative process, together with the construction of cross sections, four roughly north-south, strike-parallel sections were also constructed (Fig. 7), as was a map of the basal thrust (Fig. 8). Below, in subsection 3.2.2, we present a detailed description of our structural interpretations and explain the reasoning behind choices that were made in making them.

There are a number of uncertainties involved in the data set used to build the structural model presented below. The primary data set for the interpretation of the structure is the geological map. During the mapping a number of assumptions were made that could have led to errors in the final map. Of these, the two most important are, 1) the assumption of a chronostratigraphic correlation that links different rock units together on the basis of age and, 2) the assumptions made for correlating thrusts and stratigraphic contacts along strike through steep, heavily forested terrain with sparse outcrop. Over most of the map area, we estimate that the location of stratigraphic contacts and faults are accurate to with 1 km. Any errors generated during the mapping were then introduced into

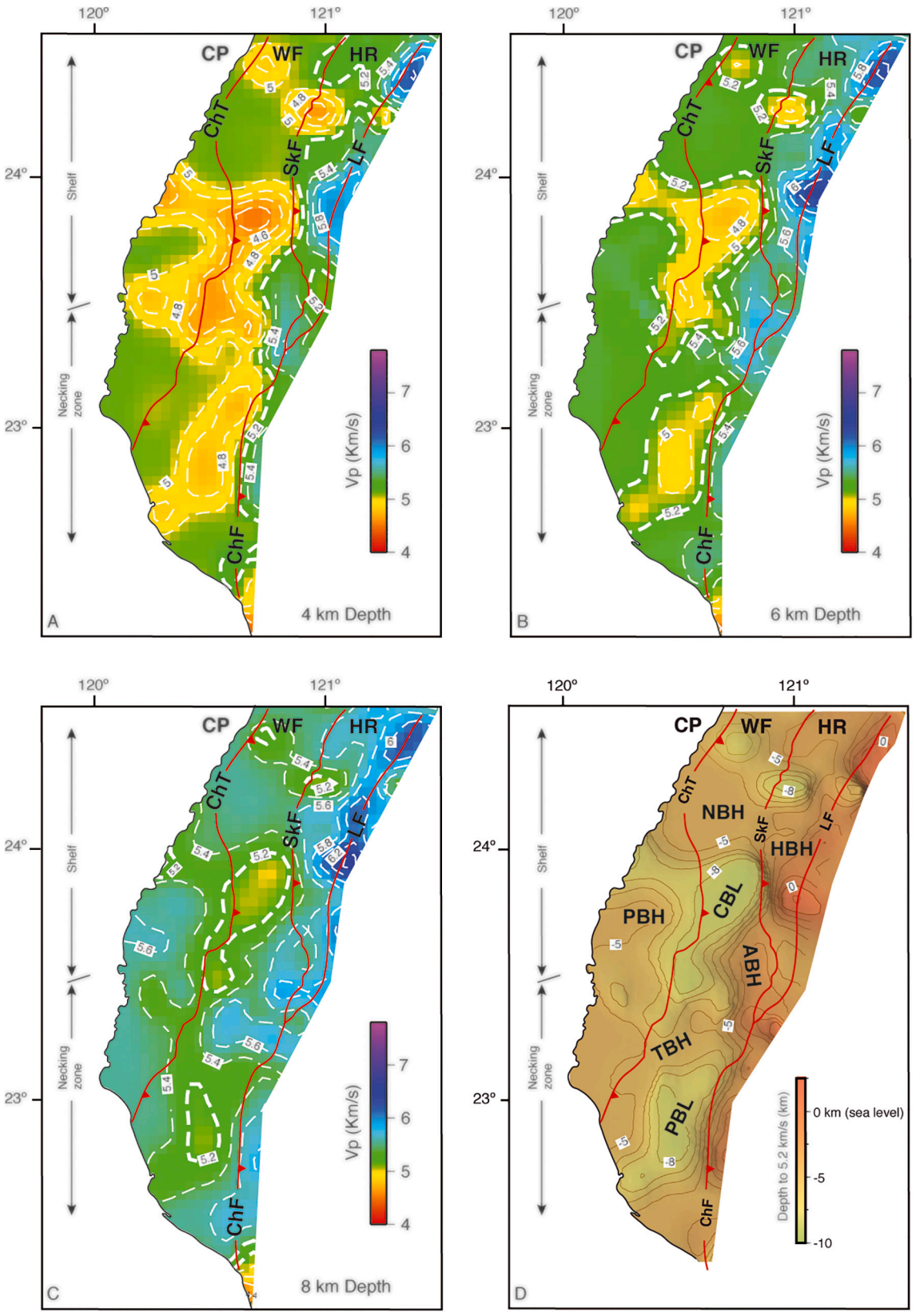

Fig. 4. A, B, and C) Vp slices at 4, 6, and 8 km depth in the study area. D) Depth to Vp = 5.2 km/s isovelocity surface that we use as a proxy for the crystalline basement – cover interface. CP = Coastal Plain, WF = Western Foothills, HR = Hsuehshan Range, ChT = Changhua Thrust, SkF = Shuilikeng Fault, LF = Lishan Fault, ChF = Chaochou Fault. NBH = Northern Basement High, HBH = Hsuehshan Basement High, PBH = Peikang Basement High, ABH = Alishan Basement High, TBH = Tainan Basement High, CBL = Central Basement Low, PBL = Pingtung Basement Low.

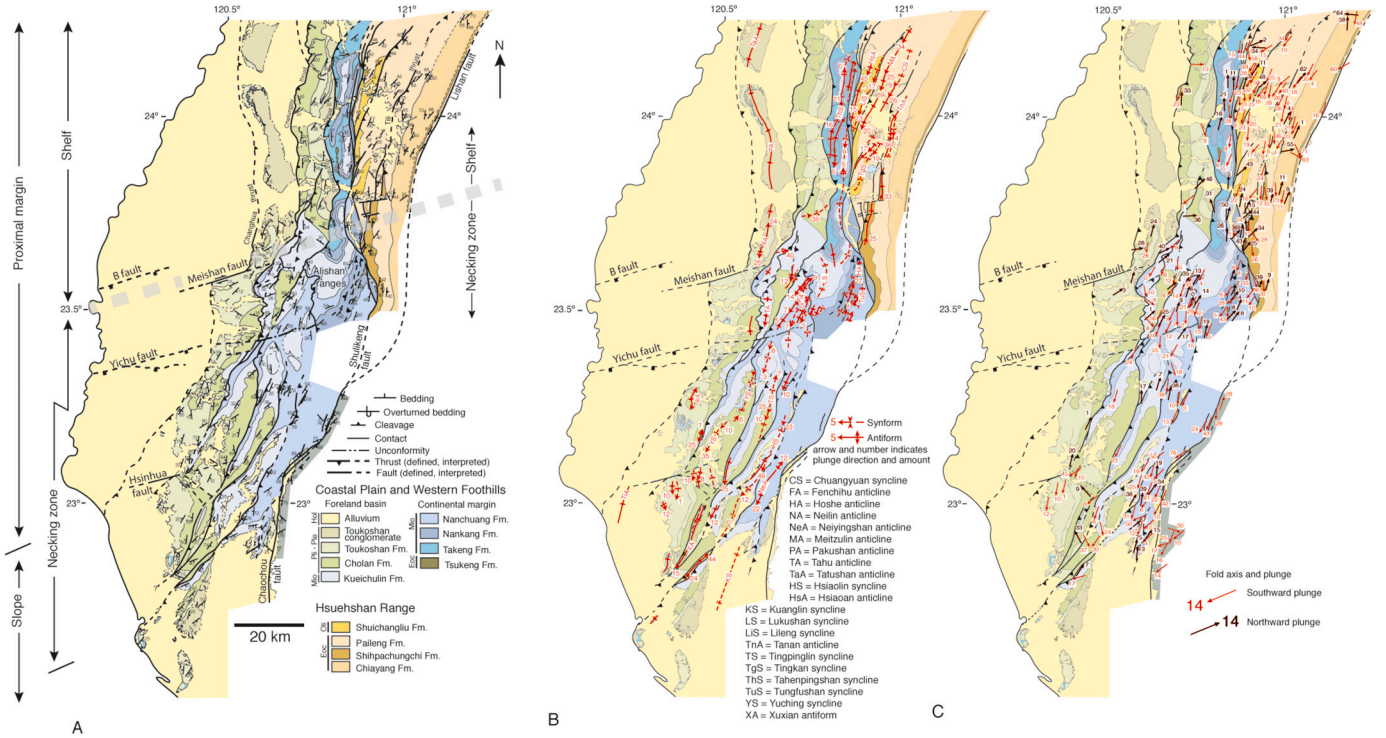

Fig. 5. A) Surface geology map of the study are with representative bedding and cleavage strikes and dips. The thick, dashed, gray line is the approximate location of the shelf to necking zone transition. B) Axial traces and plunge amount of the major antiforms and synforms. C) Representative minor fold axes and plunge amounts throughout the study area.

the cross sections and these, together with the general assumptions involved in the cross section construction (plane strain, no layer parallel slip, fold mechanism, horizontal top for the Kueichulin Fm, the depth to the basal thrust calculations) may also lead to errors in the cross sections. A weakly constrained stratigraphic thickness template precluded doing rigorous area balancing. Also, the borehole information was taken from various publications and it may, therefore, contain significant errors that we are unaware of. While we have taken care to keep all of these uncertainties to a minimum, we nevertheless present both the map and the cross sections as interpretations, the restorations as approximations, and the displacement and shortening calculations as minimums.

3.2.2. Surface geology, cross sections, basal thrust, and shortening

The surface geology of the south-central Taiwan fold-and-thrust belt is comprised of Eocene through Pleistocene clastic rocks and Holocene sediments (Fig. 5A). On the shelf area of the margin (north of the thick, gray, dashed line in Fig. 5A), thrusts and fold axial traces in the Coastal Plain and the Western Foothills strike approximately N-S, and both major and minor folds plunge (overall) gently (<20°) to moderately (20° to 40°) southward (Fig. 5B and C). Eastward, in the Hsuehshan Range, thrusts and fold axes strike roughly NNE, oblique to the Shuilikeng fault. Folds plunge predominantly to the SSW, except in the southernmost part where they often have a moderate NNE plunge (Fig. 5B and C). A penetrative, ESE-dipping pressure solution cleavage is developed in the hanging wall of the Tili thrust (Fig. 5A). Southward, the Tili thrust is cut by the Shuilikeng fault. The Hsuehshan Range is bound to the east by the Lishan fault, a ductile shear zone with an indeterminate sense of shear. South of c. 23.5° N, at the transition into the necking zone of the margin (Figs. 1 and 5), there is a marked increase in the map distribution and thickness of the Miocene rocks. Thrusts pass through a pronounced NE-striking, en-echelon bend before taking on a NNE strike farther south, and folds plunge overall toward the NE to SW (Fig. 5). The ENE-striking, dextral Meishan fault offsets the frontal thrust and minor dextral strike-slip faults are found along its strike, in the Hsuehshan Range. The map trace of the Meishan fault marks the surface rupture of the 1906 Meishan earthquake (e.g., Bonilla, 1975). The Alishan ranges (Fig. 5) are comprised of Miocene and Pliocene-aged rocks that are open to tightly folded into NNE to SSW-plunging anticlines and synclines. The southern flank of the Alishan ranges is cut by the Yichu fault, a roughly ENE-striking brittle fault zone with a dextral sense of displacement. Immediately south of the Yichu fault, thrusts have a right-stepping, en-echelon change in strike with, locally, short hanging wall splays. The structure is dominated by thrust-bound, moderately SSW-plunging synclines (Fig. 5) that are cored by syn-orogenic Pliocene and Pleistocene-aged rocks and have middle Miocene Nanchuang Fm rocks along their western limbs, in the hanging wall of thrusts. To the east, the Neiyingshan anticline (NeA) plunges moderately NNE and SSW, changing along strike into the upright Kuanglin syncline (KS). At c. 23° N, the ENE-striking, dextral Hsinhua fault can be traced from its 1946 surface rupture (e.g., Bonilla, 1975) on the Coastal Plain eastward into the thrust belt where it is associated with en-echelon bends in thrusts and ENE-striking minor faults. To the south of c. 23° N, the outcropping geology is comprised of piggyback basins carrying Holocene sediments and the Pliocene and Pleistocene rocks of the SSW-plunging Xuxian antiform (XA) (Fig. 5). In the south, the fold-and-thrust belt is bound to the east by the Chaochou fault, a brittle fault with a variable, oblique, top-to-the-northwest sense of displacement (see also Wiltschko et al., 2010).

In cross section, we interpret the structure of the south-central Taiwan fold-and-thrust belt to be a west-verging, imbricate thrust system in which listric thrusts are linked to a single basal thrust (Fig. 6). In cross sections 1, 2, and 3, on the basis of bedding dips and the thickness of the Pliocene and younger rocks in the hanging wall, we interpret the basal thrust to dip about 6° to the ENE at a depth of c. 6 to 8 km. The interpretation and location of a hanging wall flat geometry in the Changhua (ChT) and Chelungpu (CT) thrust sheets is based on published seismic reflection profiles (Wang et al., 2002), bedding dips, and the continuous outcrop of lower Pliocene rocks along the hanging wall of the

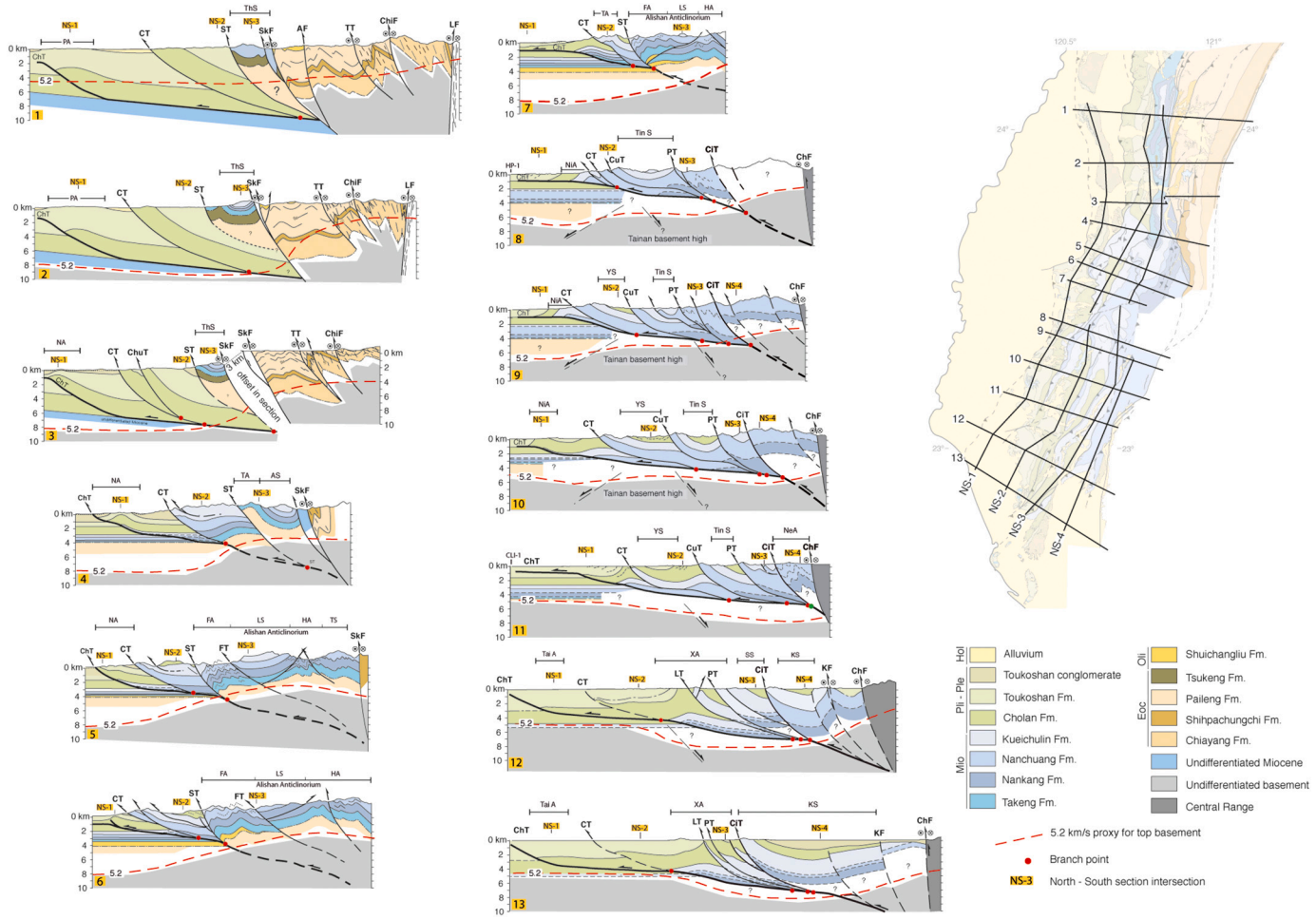

Fig. 6. Geological cross sections through the study area. The locations are shown in the inset. The 5.2 km/s velocity surface (proxy for the basement-cover interface) is shown by the dashed, red line. The intersections with the strike-parallel section in Fig. 7 are shown. ChT = Changhua Thrust, CT = Chelungpu Thrust, ChuT = Chusiang Thrust, ST = Shuangtung Thrust, FT = Fengshan Thrust, SkF = Shuilikeng Fault, AF = Alenkeng Fault, TT = Tili Thrust, ChiF = Chiayang Fault, CuT = Chutochi Thrust, PT = Pingshi Thrust, CiT = Chishan Thrust, LT = Lungchuan Thrust, KF = Kuanlin Fault, LF = Lishan Fault, ChF = Chaochou Fault. Antiform and synform abbreviations are given in Fig. 5B. (For interpretation of the references to colour in this figure legend, the reader is referred to the web version of this article.)

Table 1
Displacement and shortening values for the various thrusts in the south-central Taiwan fold-and-thrust belt. Fault abbreviations are as in Fig. 6.

	Thrusts										
Cross-section	ChT	CT	ST	SkF	CuT1	CuT2	PT	PT2	CiT	Total displacement (km)	Shortening (km)
1	1	>10	>10							>21	
2	1	>10	>10							>21	
3	4	>10	>10							>24	
4	3	4	4							11	15
5	4	7	1							12	
6	2	5	2							9	15
7	3	4	2							9	
8	7	6			9		4.5			26.5	18
9	6	10			3.5	4	4			27.5	25
10	2.5	7			5		2			16.5	17
11	1.5	3.5			5		3.5			13.5	22
12	1	2.5		7.5	7.5		3	1	3	25.5	24
13	1	3.5		5	2.5		2.2		7	21.2	16

Chelungpu thrust in this area (Fig. 5A). The Shuangtung thrust (ST) places folded lower and middle Miocene rocks on top of Pliocene and Pleistocene rocks and this, together with the hanging wall ramp structure, indicates that the basal thrust cuts down through the stratigraphy. The Shuangtung thrust sheet is bound to the east by the Shuilikeng fault (SkF). Kinematic indicators observed along the Shuilikeng fault suggest that it has a varied slip history that, when combined with earthquake focal mechanisms, indicate that it is an oblique thrust (Camanni et al., 2014b). On the basis of the obliquity of the hanging wall stratigraphic contacts and fold axial traces with the map trace of the Shuilikeng fault and the truncation of the Tili thrust, we interpret it to be out-of-sequence and to cut the Shuangtung thrust at depth (see sections 2 and 3). The outcropping Eocene and Oligocene rocks in the Hsuehshan Range indicates that the basal thrust has ramped down stratigraphic section, and

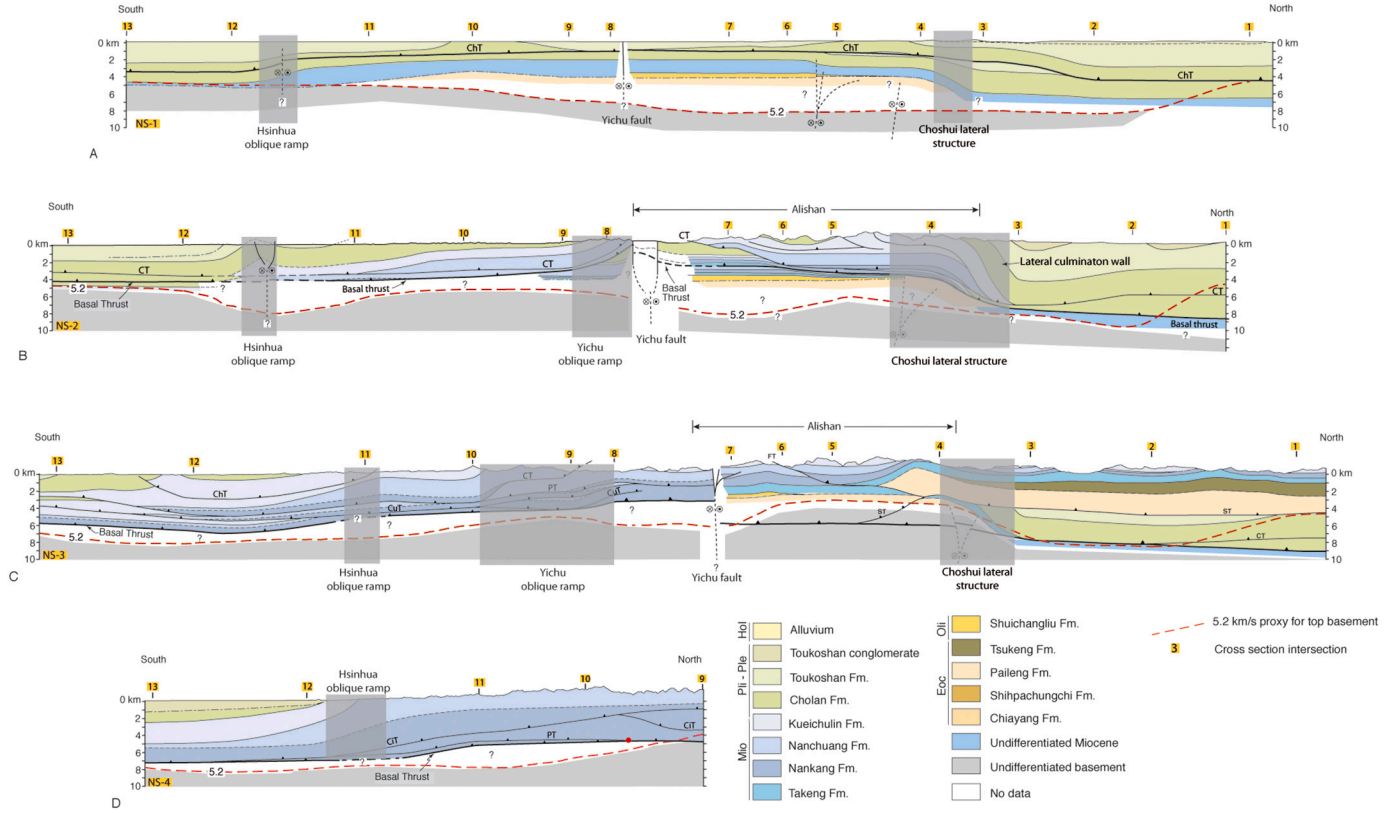

Fig. 7. Strike-parallel geological sections through the fold-and-thrust belt. The locations are shown in the inset of Fig. 6. The intersection with the cross section is shown. The 5.2 km/s velocity surface (proxy for the basement-cover interface) is shown by the dashed, red line. Fault and thrust abbreviations are as in Fig. 6. (For interpretation of the references to colour in this figure legend, the reader is referred to the web version of this article.)

the presence of rocks with a Vp >5.2 km/s in the shallow subsurface suggests that it involves crystalline basement (Figs. 4, 5 and 6). The regional-scale structure of the Hsuehshan Range is that of a northwest-verging, SSW-plunging, basement-cored anticlinorium. The combined fault displacement in sections 1 through 3 is >21 km but, because there are no stratigraphic cut-offs to the west of the Shuangtung thrust, it is not possible to calculate displacement or shortening exactly (Table 1).

Between sections 3 and 4, there is a roughly 2 km southward decrease in the thickness of the Pliocene and younger rocks, and a > 3 km increase in the thickness of Miocene rocks (Figs. 6 and 7). There is a significant north to south change in the elevation of the contact between the Kueichulin and Cholan Fms, suggesting that it is uplifted by up to 7 km (e.g., Alvarez-Marron et al., 2014). The basal thrust undergoes a pronounced change in strike, and a southward decrease in depth while ramping down stratigraphic section (Figs. 6 and 7). All of these changes between sections 3 and 4, together with the change in strike of thrusts, in the regional strike and dip of bedding, and in the plunge direction of folds, are associated with a roughly NNW-facing lateral culmination wall that we interpret to be forming due to the dextral strike-slip reactivation of an ENE-striking basement fault (Alvarez-Marron et al., 2014) (Fig. 7). We call this the Choshui lateral structure. Southward, in cross sections 4 through 7, the basal thrust has a ramp-flat geometry as it cuts down stratigraphic section from the near surface to about 4 km depth, from where it is interpreted to dip into the basement rocks (Vp >5.2 km/s) (Fig. 6). Through the Alishan ranges, the Changhua and Chelungpu (CT) thrust sheets form east-dipping monoclines with the Chelungpu thrust sheet now carrying roughly 5 km of Miocene rocks. The hanging wall of the Shuangtung thrust is comprised of several anticlines and synclines that together make up the regional-scale, west-verging, basement-cored Alishan anticlinorium. In the strike-parallel sections (Fig. 7), the Changhua and Chelungpu thrusts ramp gently up through the stratigraphic section through the Alishan ranges, with the overall geometry of hanging wall flats above footwall flats. Total fault displacement in sections 4 through 7 is between 9 and 12 km, with shortening about 15 km (Table 1). Between sections 7 and 8, across the Yichu fault, the Alishan anticlinorium changes abruptly southward to three thrust-bound synforms (Figs. 5 and 6). The Yichu fault is interpreted to breach the basal thrust (Fig. 7). In sections 8 through 13, the basal thrust has a ramp-flat geometry and dips overall about 6° toward the SE before involving basement along the eastern flank of the fold-and-thrust belt (Fig. 6). Continuously outcropping Nanchuang Fm along the hanging walls of the Chelungpu, Chutochi (CuT), and Pingshi (PT) thrusts, together with a similar level of erosion in the cores of the synclines (Fig. 5A), indicates that the basal thrust beneath these thrust sheets forms a flat within the middle Miocene rocks (Fig. 6). In sections 12 and 13, the Xuxian antiform (XA) forms a ramp anticline whose hinge and back limb areas are imbricated along the Lungchan (LT), Pingshi, and Chishan thrusts. In the strike-parallel sections (Fig. 7), the basal thrust deepens toward the south and is interpreted to be cut by Hsinhua fault. Total fault displacement in sections 8 through 13 is between 16 and 25 km, with shortening of between 15 and 25 km (Table 1).

In map view, the basal thrust has an overall c. 55° change in dip direction from north to south, and three significant changes in dip amount and dip direction that we interpret to be associated with lateral and oblique ramps (Fig. 8A). These lateral and oblique ramps are interpreted to be forming as a result of reactivation of ENE-striking faults in the basement (Alvarez-Marron et al., 2014; Camanni et al., 2016; Brown et al., 2017; Biete et al., 2018) that can be traced from the offshore through the Coastal Plain (Lin et al., 2003) and into the fold-and-thrust belt (Fig. 1A). Where basement is involved in the thrusting, the basal thrust has a steep ESE dip. Changes in the strike of the contours of the basal thrust across the Choushui lateral structure and the Yichu and Hsinhua oblique ramps, as well as the ramp into the basement beneath the Hsuehshan and Alishan ranges correlates with highs in the

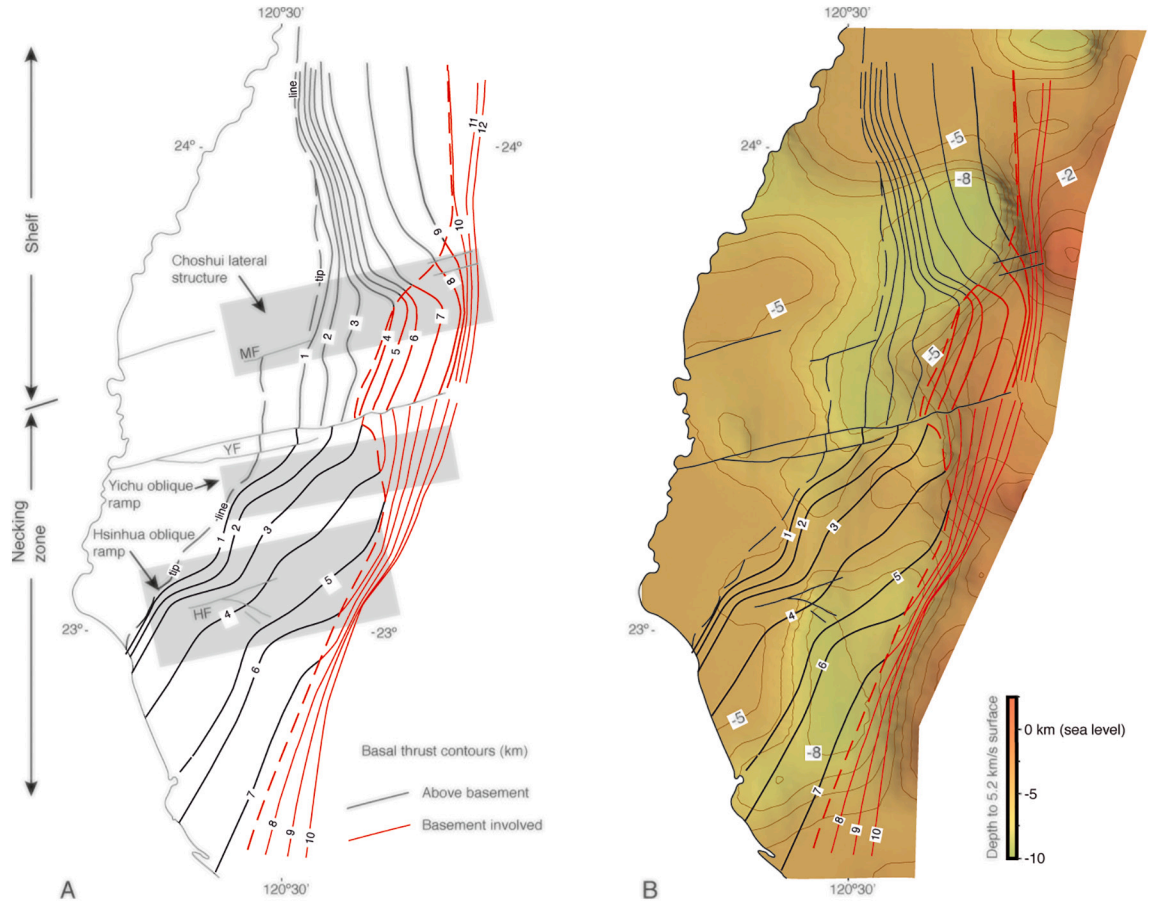

Fig. 8. A) Map of the contours (in km) of the basal thrust determined from the cross and strike-parallel sections shown in Figs. 6 and 7. Contours marked in red indicate where basement is involved in the thrusting. MF = Meishan fault, YF = Yichu fault, HF = Hsinhua fault. B) Map of the basal thrust superimposed on the 5.2 km/s proxy for the depth to the basement-cover interface. Note the correlation of the interpretation of basement involvement in the thrusting and basement highs along the eastern flank of the fold-and-thrust belt. (For interpretation of the references to colour in this figure legend, the reader is referred to the web version of this article.)

5.2 km/s isovelocity surface (Fig. 8B).

4. Proof of concept

In this section, we use a proof of concept approach to test the viability of our interpretation of the reactivation of faults inherited from the continental margin, and basement involvement in the thrusting to explain patterns of seismicity and fault type, GPS derived displacement directions and strain rates, and topography of the south-central Taiwan fold-and-thrust belt. To do this, we use the 5.2 km/s isovelocity surface proxy for the basement-cover interface and the map of the basal thrust as reference frames.

4.1. Seismicity, GPS, and topography data

4.1.1. Seismicity

Earthquake hypocenter data from 1994 through 2014 (Fig. 9) was relocated using the double-difference technique (Waldhauser and Ellsworth, 2000) within the 3D Vp model of Kuo-Chen et al. (2012) using the HypoDD3D software (Waldhauser, 2001). The relocation was carried out on all events shallower than 25 km depth that had a minimum of six readings with a reading weighting <3 (good quality). The average horizontal and vertical uncertainties in earthquake locations are estimated to be ±1 km and ± 2 km, respectively, although these uncertainties could be larger (see Wu et al., 2008a; Chen et al., 2017). Within the study area, focal mechanisms were calculated from first motion polarities of P waves (Wu et al., 2008b) for 2465 events with magnitudes between 1.4 to 6.8 M_L. Fault types (Fig. 10) were calculated using the classification scheme of Zoback (1992).

In the 4 km and 6 km depth slices, seismicity is taking place above and along the basal thrust, although some clusters in its hanging wall extend into the footwall and the basement below (Fig. 9). In the 4 km and 8 km depth slices, seismicity is taking place above the basal thrust where basement is involved in the thrusting. At depths to 16 km, there is a marked increase in seismicity from north to south across the Choshui lateral structure (CLS), with well-developed hypocenter clusters along the western flank of the Alishan Basement High (ABH), in the southern part of the Central Basement Low (CBL), and in the northern part of the Pingtung Basement Low (PBL). There are very few events around the Peikang Basement High (PBH). There is a significant west to east increase in seismicity into the Hsuehshan Basement High (HBH), with the crust being seismically active to a depth of >20 km. South of the Choushui lateral structure, scattered seismicity extends west of the interpreted tip line of the basal thrust to a depth of 20 km.

Thrust and strike-slip fault types are the most common in the study area, with lesser transpressional and rare extensional faulting also taking place (Fig. 10). Strike-slip is the most common fault type to the west of the tip line of the basal thrust and both above and below the basement-cover interface. Strike-slip is also the most common fault type in the upper 5 km throughout the study area, and in the upper 10 km along the eastern flank of the thrust belt. Along the Choshui lateral structure, in the 5 to 15 km depth range, a roughly ENE-striking cluster of strike-slip fault types is located predominantly below the basement-cover interface and below the basal thrust. Between the Choshui

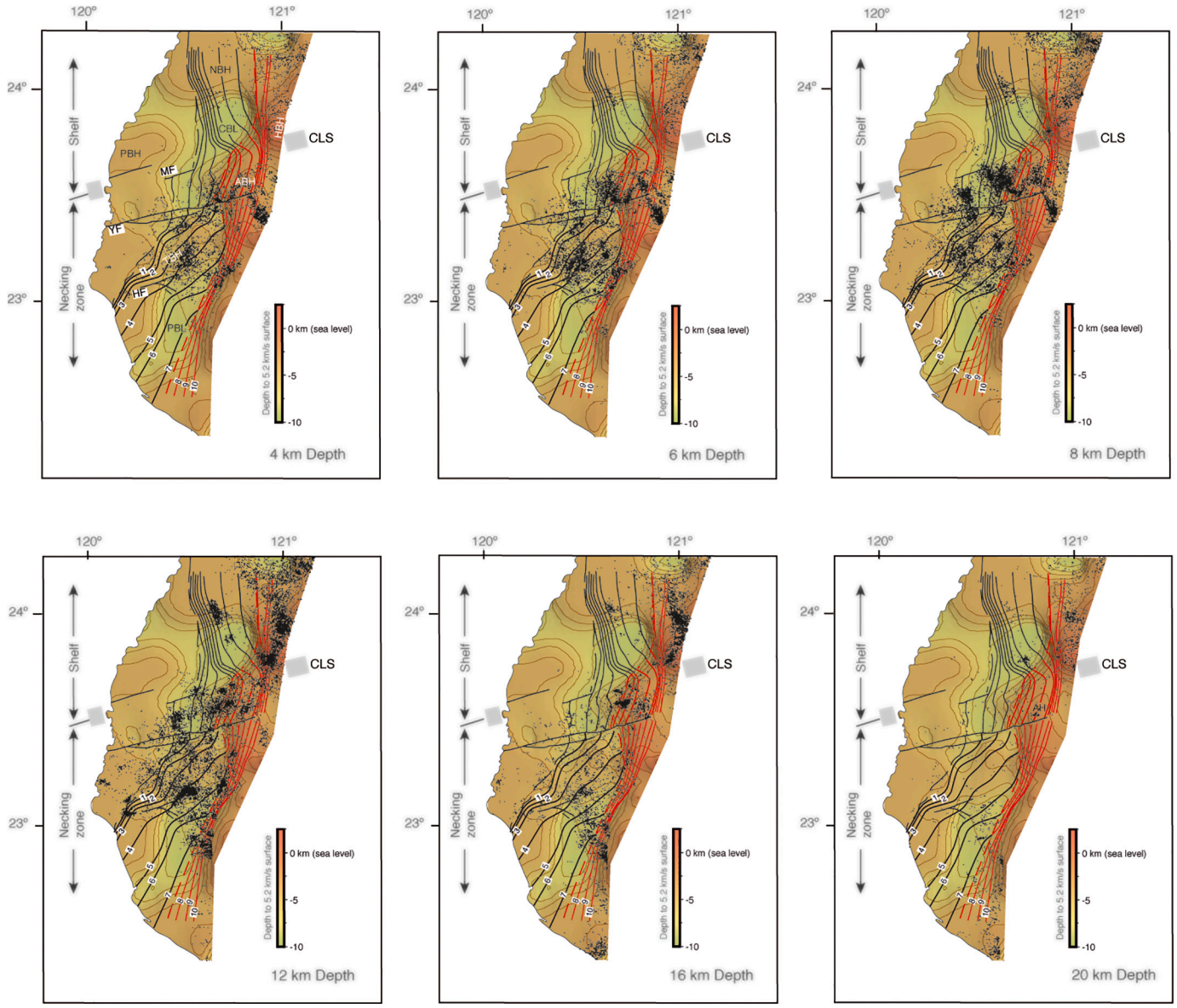

Fig. 9. Depth slices of earthquake hypocenters superimposed on the 5.2 km/s proxy for the basement-cover interface and the contour map of the basal thrust. In the 4, 6, and 8 km slices hypocenters are project 0.99 km on either side, whereas in the 12, 16, and 20 km slices they are projected 1.99 km. Basement highs and lows are labeled as in Fig. 4. The ENE oriented gray label is the Choshui Lateral Structure (CLS). Fault labels are as in Fig. 8.

lateral structure and the Yichu fault (YF), at this depth range thrust fault types are common near and below the basement-cover interface and below the basal thrust. Along the Yichu fault, strike-slip is the most common fault type in the upper 20 km, with lesser thrust fault types to a depth of 15 km. South of the Yichi fault, at 0 to 10 km depths, scattered thrust and strike-slip fault types occur throughout the area of the Tainan Basement High (TBH), whereas at 10–15 km depth thrust clusters occur along its southern and eastern flank and strike-slip along the west. Both fault types are mostly concentrated below the basement-cover interface and the basal thrust. Along the eastern flank of the thrust belt, where basement is involved in the deformation, strike-slip fault types are common in the upper 10 km, with thrust types becoming more common with increasing depth.

4.1.2. GPS measurements in the south-central Taiwan fold-and-thrust belt

GPS data from 2005 through 2009 was used to calculate horizontal displacement vectors, maximum shear strain, and vertical rotation rate using the SSPX software of Cardozo and Allmendinger (2009) (Figs. 11). The GPS data were processed using the method of Yu et al. (1997) and the reader is referred there for details. Horizontal velocities were calculated relative to station S01R located on the island of Penghu in the Taiwan Strait (Fig. 1). Maximum shear strain and vertical rotation rate were calculated using a 5 × 5 km grid and a grid-nearest neighbour interpolation method using the 10 nearest stations within a maximum radius of 35 km.

In the west of the study area, there is an abrupt eastward increase in the horizontal displacement velocity, although there is little apparent relationship with the shape of the basement-cover interface (Figs. 11A). Relative highs in the maximum shear strain and vertical rotation rate take place along the margins of the basement highs and lows, especially the southern part of the NBH, the western margin of the HBH, and the western margin of the PBL (Fig. 11B, C). There are clear changes in the horizontal displacement vectors, maximum shear strain, and vertical rotation rate relative to the ENE-striking faults that breach the basal thrust (Figs. 11D, E, and F). North of the Choshui lateral structure (CLS), displacement is toward the WNW, whereas southward there is a c. 10°

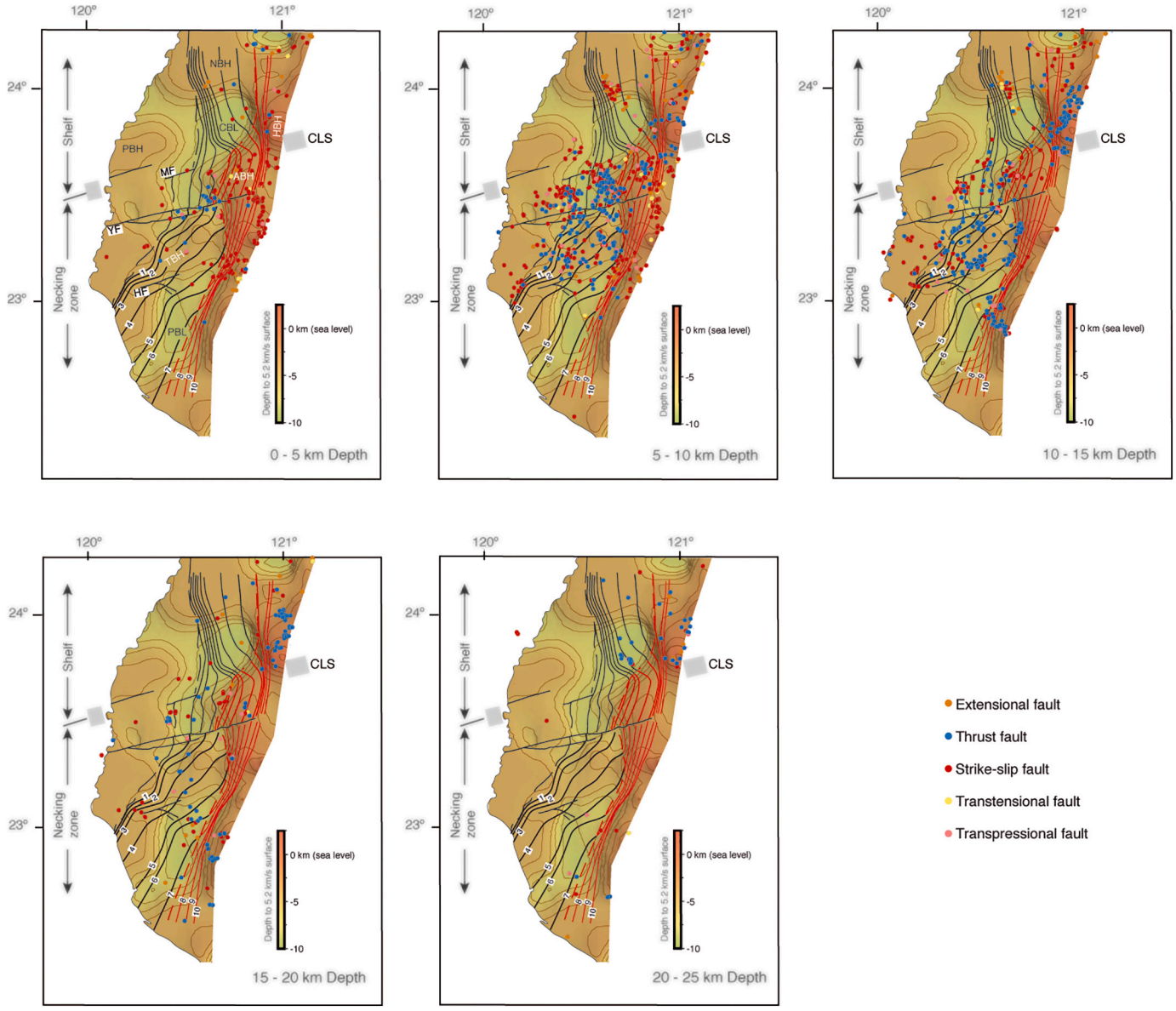

Fig. 10. Depth slices with fault types calculated from focal mechanisms superimposed on the 5.2 km/s proxy for the basement-cover interface and the contour map of the basal thrust. Hypocenters are projected from within the depth range indicated in each slice. Basement highs and lows are labeled as in Fig. 4. The ENE oriented gray label is the Choshui Lateral Structure (CLS). Fault labels are as in Fig. 8.

counter-clockwise rotation of displacement directions, an increase in maximum shear strain, and a change in the sense and in the magnitude of the vertical rotation rate (Fig. 11 D, E, and F). South of the Yichu fault (YF), there is a further 10° to 15° counter-clockwise rotation of the horizontal displacement directions and a gradual increase in velocities. This is accompanied by an increase in the maximum shear strain and a marked increase in the vertical rotation rate. South of Hsinhua fault at c. 23° N, displacement is toward the southwest, there is a sharp, local increase in the maximum shear strain, and the vertical rotation rate changes from clockwise to counter-clockwise.

4.1.3. Topography of the south-central Taiwan fold-and-thrust belt

A 40-m pixel digital elevation model was used to investigate whether or not there is any relationship between the topography of the fold-and-trust belt, the basement-cover interface, and the geometry of the basal thrust and (Fig. 12).

Throughout the south-central Taiwan fold-and-thrust belt, there is a good correlation between high topography and basement highs, with the highest topography above the Hsuehshan (HBH) and Alishan (ABH) highs, and lower topography across the Tainan (TBH) and Northern (NBH) highs (Fig. 12A). There is no high topography associated with the Peikang Basement High (PBH). The high topography along the eastern margin of the fold-and-thrust belt is developed above the area where basement is involved in the thrusting (Fig. 12B). Across the Choshui lateral structure (CLS), there is a roughly ENE-striking, north to south increase in topography of >2000 m into the Alishan ranges that coincides with the NNW-facing Choshui lateral culmination wall (Fig. 7). Similarly, but with lesser effect, there is a clear topographic signature associated with the Yichu fault. South of the Yichu fault (YF), the topography is comprised of southward-plunging, long, narrow, curved ridges that correlated with changes in strike of thrusts across the Yichu (YOR) and Hsinhua (HOR) oblique ramps.

4.2. Testing the viability of the model

In our model of the structure of the south-central Taiwan fold-and-

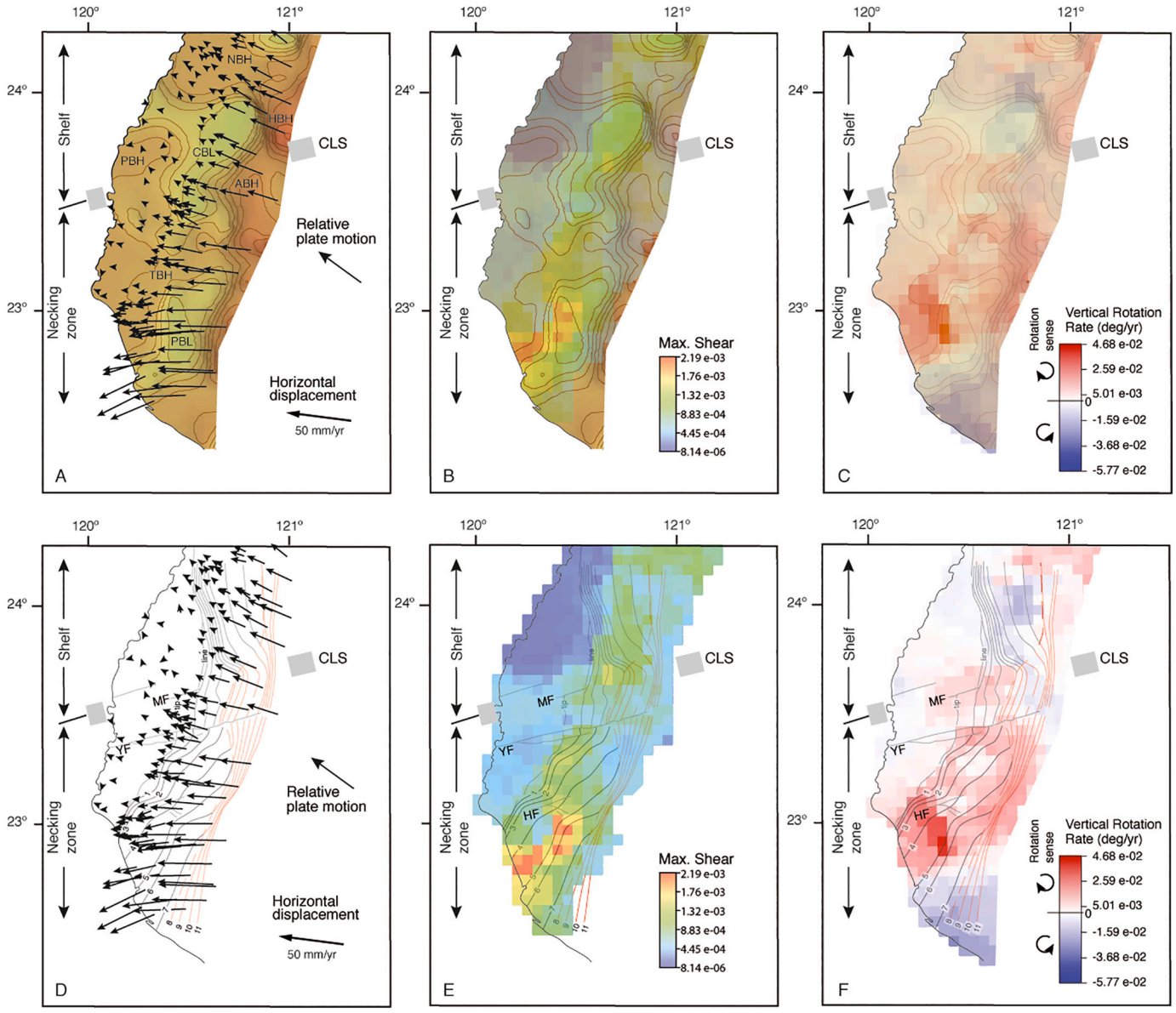

Fig. 11. A) GPS displacement vectors, B) maximum shear strain, and C) vertical rotation rate superimposed on the depth to the 5.2 km/s proxy for the basement-cover interface. Basement highs and lows are labeled as in Fig. 4. D) GPS displacement vectors, E) maximum shear strain, and F) vertical rotation rate superimposed on the map of the basal thrust. Basement highs and lows are labeled as in Fig. 4. CLS = Choshui Lateral Structure. Fault labels are as in Fig. 8.

thrust belt (i.e. Alvarez-Marron et al., 2014; Camanni et al., 2016; Brown et al., 2017; Biete et al., 2018), fault reactivation is taking place along a Miocene-aged ENE-striking extensional fault system that has been traced from offshore in the Taiwan Strait into the Coastal Plain of southwestern Taiwan (Chang, 1963, 1964; Lin et al., 2003; Yang et al., 2016). In the model, reactivation of this fault system is responsible for the along-strike changes across the Choshui lateral structure, and the Yichu and Hsinhua faults. We suggest that much of the seismicity below the basal thrust can be explained by slip along ENE-striking faults that bound basement highs and lows inherited from the margin. These faults are favorably orientated for strike-slip and transpressional reactivation in the contemporaneous stress field of southwest Taiwan (e.g., Suppe, 1995; Lacombe et al., 1999; Mouthereau and Lacombe, 2006; Mouthereau et al., 2009; Biete et al., 2019), which can explain the widespread occurrence of this fault type in the focal mechanism data. Our interpretation that these reactivated faults breach the basal thrust and affect the surface deformation of the fold-and-thrust belt can explain the variations observed in the GPS displacement directions, shear strain rate, and vertical rotation rate that takes place across the Choshui lateral structure, the Yichi fault, and the Hsinhua fault. SW-directed displacement and high strain rates in the southwest can possibly be explained by slip taking place along the Hsinhua oblique ramp, which is forming along the flank of the Pingtung Basement Low (Fig. 8B). Our model is less successful, however, in explaining the seismicity above the basal thrust, except along the eastern flank of the fold-and-thrust belt where it is interpreted to ramp down into the crystalline basement. This interpretation of a ramp in the basal thrust can explain the deepening of seismicity in these areas (Alvarez-Marron et al., 2014; Camanni et al., 2016; Brown et al., 2017; Biete et al., 2018) and the oblique displacement mapped along the Shuilikeng, Lishan, and Chaochou faults (see also, Lee et al., 1997; Wiltschko et al., 2010; Camanni et al., 2014b; Kuo-Chen et al., 2015) can explain the distribution of strike-slip and thrust fault types in the Hsuehshan and Alishan ranges. Our interpretation that the basal thrust ramps down into the crystalline basement also explains the development of high topography (see also, Mouthereau et al., 2002), a relationship also found in other mountain belts (e.g., Kley et al., 1996;

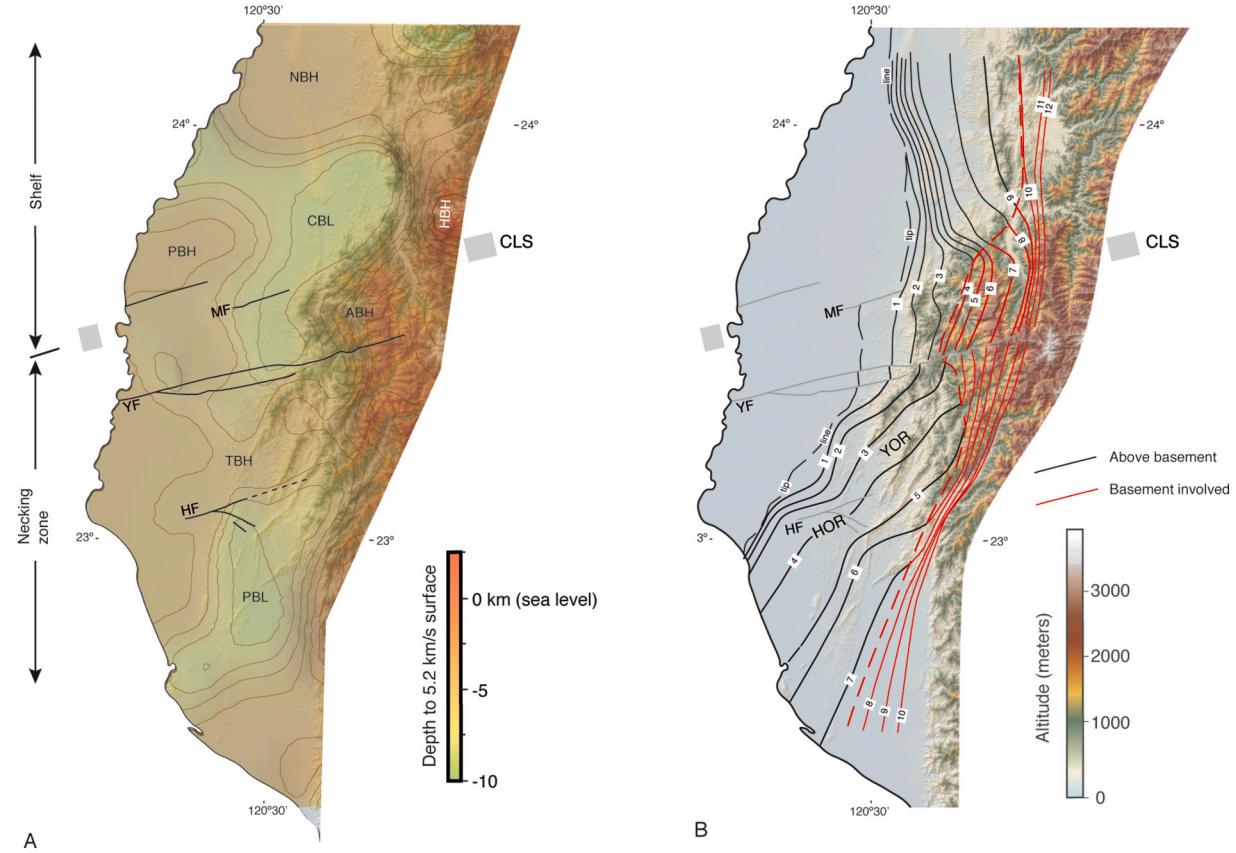

Fig. 12. A) Topography of the study area superimposed on the depth to the 5.2 km/s proxy for the basement-cover interface. Basement highs and lows are labeled as in Fig. 4. B) Topography of the study area superimposed on the map of the basal thrust. CLS = Choshui Lateral Structure. Note that, along the eastern flank of the fold-and-thrust belt, there is a good correlation between high topography, basement highs, and basement involvement in the thrusting. Fault labels are as in Fig. 8.

Mouthereau et al., 2006; Pfiffner, 2017).

On the basis of the proof of concept analyses presented in this section, we suggest that our interpretations of along-strike changes being caused by the reactivation of ENE-striking faults inherited from the margin and of basement involvement in the thrusting are viable since they can explain the first-order patterns of seismicity, GPS displacement vectors and strain rates, and topography data. We stress, however, that other models (e.g., Wu et al., 1997; Mouthereau et al., 2009; Ching et al., 2011) may also explain these data sets and can therefore be considered viable.

5. Discussion

Although there are important differences between the many structural models for the south-central Taiwan fold-and-thrust belt (e.g., Suppe, 1980, 1981, 1986; Mouthereau et al., 2001; Hickman et al., 2002; Yue et al., 2005; Mouthereau and Lacombe, 2006; Yang et al., 2007, 2016; Rodriguez-Roa and Wiltschko, 2010), most authors, including us (e.g., Brown et al., 2012, 2017; Alvarez-Marron et al., 2014; Camanni et al., 2014a, 2016; Biete et al., 2018), interpret it to be an imbricate thrust system. The major differences between the models revolve around, 1) the location and nature of the basal thrust, 2) whether or not there are transverse structures and if so, what is causing them, 3) whether or not there is basement involvement in the thrusting, 4) the amount of shortening and, 5) the structure of the Hsuehshan Range.

The basal thrust is a key structure in the interpretation of any fold-and-thrust belt, since its geometry and location (depth) has important implications for the deformation style, the mechanics, and the involvement (or not) of basement in the deformation (e.g., Davis et al., 1983; Judge and Allmendinger, 2011; Poblet and Lisle, 2011; Pfiffner, 2017; Lacombe and Bellahsen, 2016; Tavani et al., 2021). Therefore, a map of the basal thrust, even with its uncertainties, is an important tool for understanding the structure of a fold-and-thrust belt (e.g., shortening, basement involvement) and how (or if) it is affected by activity in its footwall (e.g., fault reactivation and the formation of transverse zones). In this paper, we have used new geological surface mapping, serial cross-sections, strike-parallel sections, and a proxy for the basement-cover interface to map the location and geometry of the basal thrust throughout the south-central Taiwan fold-and-thrust belt (Fig. 8). Most other interpretations of the basal thrust in this area are 2D (cross section), with the exception of Huang et al. (2004) and Carena et al. (2002) who map parts of its surface. Our proposal for the geometry and depth of the basal thrust (Fig. 8) differs from that of Hung et al. (1999), Mouthereau et al. (2001, 2002), Carena et al. (2002), Hickman et al. (2002), Yue et al. (2005), Yang et al. (2007, 2016), and Rodriguez-Roa and Wiltschko (2010) who interpret it to be deeper than in our model, or even that there are two levels of detachment. Lacombe and Mouthereau (2002) and Mouthereau and Lacombe (2006) suggest that there may even be a deep, ductile detachment. Furthermore, we interpret the basal thrust to ramp down into the middle crust along the eastern flank of the fold-and-thrust belt, unlike Suppe (1980, 1981), Carena et al. (2002), Yue et al. (2005), and Malavieille and Trullenque (2009) who suggest that it is a through-going detachment near the base of the sedimentary package across the entire mountain belt.

Our structural mapping allows us to interpret the presence of two well-defined ENE-striking transverse zones (the Choshui lateral structure and the Yichu fault), and one lesser one (the Hsinhua fault) (Figs. 5A and 8A). Transverse zones are defined as "a systematic alignment of lateral connectors between two sets of differing structures" (Thomas,

1990). They are *syn*-kinematic with respect to fold-and-thrust belt structures and are possibly controlled by reactivated basement faults, mechanical variations along the basal thrust, or a combination of these (Thomas, 1990). We suggest that the transverse zones identified in the south-central Taiwan fold-and-thrust belt have a causal relationship to the east-northeast striking faults that have been mapped on the margin and traced into the western Taiwan (Alvarez-Marron et al., 2014; Camanni et al., 2016; Brown et al., 2017; Biete et al., 2018, 2019). This interpretation is in agreement with that of Mouthereau and Lacombe (2006) who suggested the presence of ENE-trending structures and their relationship to basement faults. We provide a proof of concept analysis that suggests that this interpretation can explain the distribution of seismicity and fault types, GPS displacement vectors and strain rates, as well as the topography of the study area. Further support for the interpretation is provided by the dextral strike-slip surface ruptures developed during the 1906 Meishan and the 1946 Hsinhua earthquakes (Bonilla, 1975; Shyu et al., 2005, 2016). Nevertheless, a number of other studies (e.g., Deffontaines et al., 1997; Lacombe et al., 1999; Mouthereau et al., 1999, 2002) have suggested that several roughly NW-striking transfer (sic) zones affect the structure of the Taiwan fold-and-thrust. These transfer zones were interpreted to be related to either pre-existing extensional faults in the under-thrusting margin, to deformation taking place along the margins of basement highs, or as newly formed structures in the hanging wall of the fold-and-thrust belt (e.g., Deffontaines et al., 1997; Lacombe et al., 1999; Mouthereau et al., 1999, 2002). However, NW-striking faults have not been reported from the part of the margin that is entering into the deformation in south-central Taiwan; Eocene-age rift basins having NE-striking bounding faults (Hsu, 2001; Lin and Watts, 2002; Lin et al., 2003; Teng and Lin, 2004; Lin et al., 2005), and Miocene-aged basins have ENE-striking bounding faults (Lee et al., 1993; Lin et al., 2003; Lin et al., 2005; Ding et al., 2008; Shi et al., 2008; Tang and Zheng, 2010; Yang et al., 1991, 2016; Yeh et al., 2012; McIntosh et al., 2014). Furthermore, we find no concrete evidence in our mapping to support the presence of regional, NW-striking transfer zones that affect the fold-and-thrust belt.

In the absence of other data, using a proxy of 5.2 km/s (Fig. 3) for the basement - cover interface provides a way forward for the interpretation of the involvement of crystalline basement rocks in the thrusting in the south-central Taiwan fold-and-thrust belt. The definition of basement as crystalline rocks used in this paper differs from that of other authors who generally define basement in Taiwan as any pre-Miocene rocks (e.g., Hung et al., 1999; Mouthereau et al., 2001, 2002; Lacombe and Mouthereau, 2002; Hickman et al., 2002; Lacombe et al., 2003; Huang et al., 2004; Mouthereau and Lacombe, 2006; Yang et al., 2007, 2016; Rodriguez-Roa and Wiltschko, 2010) and interpret basement involvement in the thrusting, even along the westernmost flank of the fold-and-thrust belt. As we indicate in Section 3.2.2, there is widespread evidence that the basal thrust is near the base of the Pliocene Cholan Fm in the north of the study are and within the middle Miocene Nanchuang Fm in the south, indicating that basement is not involved in the thrusting along the western part of the thrust belt. The eastern flank of the thrust belt, however, can be interpreted to involve crystalline basement (Vp >5.2 km/s), albeit with two different styles. Using the terminology of Poblet and Lisle (2011) and Pfiffner (2017), the structural style of the Hsuehshan Range can be interpreted as thick-skinned with the basal thrust ramping steeply into the basement, reactivating an Eocene-aged extensional fault to a depth of 20 km or more (see also, Brown et al., 2012; Camanni et al., 2014a, 2014b; Kuo-Chen et al., 2015), whereas the Alishan Range, with a thin sheet of crystalline basement rocks (Alvarez-Marron et al., 2014), appears to be basement-involved (Fig. 6).

In our cross section interpretations, shortening in the south-central Taiwan fold-and-thrust belt is larger in the north (> 25 km), decreasing across the Choshui lateral structure and southwards through the Alishan Ranges (c. 15 km), before increasing southward (17 to 25 km) across the Yichu fault (Table 1). Our shortening estimates are in keeping with those of between 10 km to 30 km made by Yang et al. (2006, 2007, 2016), Mouthereau et al. (2001), Hickman et al. (2002), Mouthereau and Petit (2003), Mouthereau and Lacombe (2006), and Rodriguez-Roa and Wiltschko (2010). It is, however, in sharp contrast to the interpretations of Suppe (1980, 1986) whose sections, if restored (cross sections are not restored and shortening values are not mentioned in these publications), record >87 km of shortening along our section 5, and >50 km of shortening along the frontal part of our sections 7 through 10. In our sections 7 through 10, for example, placing the basal thrust at c. 1 km to 2 km depth along the front of the thrust system and a ramp to the east (to c. 4 km depth) allows us to accommodate the surface bedding dips by interpreting a fault bend fold whose back limb is cut by a thrust. Suppe (1980) interprets a complex duplex and antiformal stack structure that involves much more shortening. Nevertheless, Suppe (1980) indicates that "…given the large number of imbrications needed to satisfy the surface dips, considerable rearrangement of the faults and decollement horizons may be possible.", and that there "…is a major problem with this provisional cross section…". We suggest that the simpler solutions presented by us and by Mouthereau et al. (2001), Mouthereau and Petit (2003), Mouthereau and Lacombe (2006), Yang et al. (2006, 2016), and Rodriguez-Roa and Wiltschko (2010) provide a more accurate interpretation of the structure and more realistic estimates of the amount of shortening.

Mapping in the Hsuehshan Range has provided extensive new structural data, including the recognition of structures cut by the Shuilikeng fault, a regional-scale anticlinorium in the hanging wall of the Tili thrust, a zone of ductile deformation along the Lishan fault, a vertical east-facing limb along the Lishan fault (Brown et al., 2012). Furthermore, our geological mapping along >100 km of the strike length of the Shuilikeng fault (e.g., Brown et al., 2012; Camanni et al., 2014b) showed it to have a complex displacement history and to truncate structures in both its footwall and hanging wall (Fig. 5), suggesting that it has a long and varied history of oblique, out-of-sequence thrusting. These structures were not recognised previously in the structural interpretations of this part of the fold-and-thrust belt. For example, Suppe (1986) interprets the Shuilikeng fault to be an east-dipping hanging wall flat that merges with a basal detachment at about 8 km depth beneath the Hsuehshan Range, whereas Mouthereau et al. (2002) interpret it (their Chushih thrust) to penetrate into the basement (which they define as any pre-Miocene rocks), but without any detachment being interpreted. Yue et al. (2005) interpret the Shuilikeng fault to be a west-dipping extensional fault that has been cut and transported westward, leaving its seismically active lower part in the footwall to the detachment. Rodriguez-Roa and Wiltschko (2010), interpret the Shuilikeng fault (their Tulungwan thrust) to extend from central Taiwan to the south where it becomes the Chaochou fault, and to merge with a basal detachment in the Miocene. Although Yue et al. (2005) interpret the surface structure of the westernmost part of the Hsuehshan Range in a similar way to us they interpret the eastern part, from the Tili thrust to the Lishan fault, to be an east-dipping monocline with the structure of a hanging wall flat, as does Suppe (1986). Neither Yue et al. (2005), nor Suppe (1986) recognise the Lishan fault. Only Clark et al. (1993) suggest that the Hsuehshan Range is a pop-up structure that inverts the extensional Hsuehshan Basin, which is in keeping with our interpretations. Other authors, such as Lin et al. (2003) and Teng and Lin (2004) do hint that tectonic inversion is taking place in the Hsuehshan Range (for example, see Fig. 3 of Lin et al., 2003), but they do not explicitly say so.

6. Conclusions

In this paper, we bring together the results of our previous studies and add new data and data analyses to develop a 3D structural model for the structure of south-central Taiwan. We interpret the fold-and-thrust belt to be a west-verging, imbricate thrust system developed above a single basal thrust that is breached by ENE-striking strike-slip to transpressive faults that are developed along the flanks of basement highs and low. These breaching faults are inherited from the continental margin

and are associated with ENE-striking transverse zones in the fold-and-thrust belt. Across these transverse zones there are changes in a combination of stratigraphy, structural style, strike and dip of the basal thrust, and uplift of the stratigraphic contacts. Along the eastern flank of the fold-and-thrust belt, the uplift of rocks with Vp > 5.2 km/s leads us to interpret crystalline basement to be involved in the thrusting. Shortening estimates range from 15 km to >25 km and varies across the transverse zones. While our proposed structural model has many similarities and differences with those of other authors, we suggest that its depth and along-strike consistency, together with is ability to explain aspects of the distribution of seismicity, faults types, GPS displacement vectors and strain rates, and topography of the study area makes it a viable model.

Declaration of Competing Interest

The authors declare that they have no known competing financial interests or personal relationships that could have appeared to influence the work reported in this paper.

Acknowledgements

This publication if part of the I+D+i project PGC2018-094227-B-I00 financed by MCIN/AEI/ https://doi.org/10.13039/501100011033 and the Generalitat de Catalunya, grant/award number AGAUR 2017SGR1022. We wish to thank two anonymous reviewers for their insightful comments on the manuscript.

Appendix A. Supplementary data

Supplementary data to this article can be found online at https://doi.org/10.1016/j.earscirev.2022.104094.

References

Alvarez-Marron, J., Brown, D., Camanni, G., Wu, Y.-M., Kuo-Chen, H., 2014. Structural complexities in a foreland thrust belt inherited from the shelf-slope transition: insights from the Alishan area of Taiwan. Tectonics 33, 1322–1339.

Biete, C., Alvarez-Marron, J., Brown, D., Kuo-Chen, H., 2018. The structure of southwest Taiwan: the development of a fold-and-thrust belt on a margins outer shelf and slope. Tectonics 37, 1973–1993. https://doi.org/10.1029/2017TC004910.

Biete, C., Brown, D., Lund, B., Alvarez-Marron, J., Wu, Y.-M., Kuo-Chen, H., Ho, C.-W., 2019. The influence of inherited continental margin structures on the stress and strain fields of the south-central Taiwan fold-and-thrust belt. Geophys. J. Int. 219, 430–448.

Bonilla, M.G., 1975. A review of recently active faults in Taiwan. USGS Open-File Rep. 75-41, 43.

Brocher, T.M., 2005. Empirical relations between elastic wavespeeds and density in the Earth's crust. Bull. Seismol. Soc. Am. 95, 2081–2092.

Brown, D., Alvarez-Marron, J., Schimmel, M., Wu, Y.-M., Camanni, G., 2012. The structure and kinematics of the Central Taiwan mountain belt derived from geological and seismicity data. Tectonics 31. https://doi.org/10.1029/2012TC003156.

Brown, D., Alvarez-Marron, J., Biete, C., Kuo-Chen, H., Camanni, G., Ho, C.-W., 2017. How the structural architecture of the Eurasian continental margin affects the structure, seismicity, and topography of the south-central Taiwan fold-and-thrust belt. Tectonics 36, 1275–1294. https://doi.org/10.1002/2017TC004475.

Camanni, G., Ye, Q., 2022. The significance of fault reactivation on the Wilson cycle undergone by the northern South China Sea area in the last 60 Myr. Earth-Sci. Rev. 225, 103893.

Camanni, G., Chen, C.-H., Brown, D., Alvarez-Marron, J., Wu, Y.-M., Chen, H.-A., Huang, H.-H., Chu, H.-T., Chen, M.-M., Chang, C.-H., 2014a. Basin inversion in Central Taiwan and its importance for seismic hazard. Geology 42 (2), 147–150.

Camanni, G., Brown, D., Alvarez-Marron, J., Wu, Y.-M., Chen, H.-A., 2014b. The Shuilikeng fault in Central Taiwan mountain belt. J. Geol. Soc. 171, 117–130.

Camanni, G., Alvarez-Marron, J., Brown, D., Ayala, C., Wu, Y.-M., Hsieh, H.-H., 2016. The deep structure of south-central Taiwan illuminated by seismic tomography and earthquake hypocentre data. Tectonophysics 679, 235–245.

Campbell, K.W., Thenhaus, P.C., Barnhard, T.P., Hampson, D.B., 2002. Seismic hazard model for loss estimation and risk management in Taiwan. Soil Dyn. Earthq. Eng. 22, 743–754. https://doi.org/10.1016/S0267-7261(02)00095-7.

Cardozo, N., Allmendinger, R.W., 2009. SSPX: a program ro compute strain from displacement/velocity data. Comput. Geosci. 35, 1343–1357.

Carena, S., Suppe, J., Kao, H., 2002. Active detachment of Taiwan illuminated by small earthquakes and its control of first-order topography. Geology 30, 935–938.

Chang, S.L., 1963. Regional stratigraphic study of Pliestocene and Upper Pliocene formations in Chiayi and Hsinying area, Taiwan. Pet. Geol. Taiwan 2, 65–86.

Chang, S.L., 1964. Regional stratigraphic study of lower Pliocene and Upper Miocene formations in Chiayi and Hsinying area, Taiwan. Pet. Geol. Taiwan 3, 1–20.

Chen, C.-H., 2000. Geological Map of Taiwan, Scale 1:500,000. Central Geological Survey, Taipei.

Chen, A.T., Yang, Y.-L., 1996. Lack of compressional overprint on the extensional structure in the offshore Tainan and the tectonic implications. Terr. Atmos. Ocean. Sci. 7, 505–522.

Chen, M.-M., Yu, N.-T., Chu, H.-T., Shea, K.-S., Hsieh, Y.-C., 2009. Larger foraminifera in the so-called "Meichi Sandstone" of Wujie area, southern Hsuehshan Range. Cent. Geol. Surv. Spec. Publ. 22, 227–242.

Chen, K.-X., Kuo-Chen, H., Brown, D., Li, Q., Ye, Z., Liang, W.-T., Wang, C.-Y., Yao, H., 2016. Three-dimensional ambient noise tomography across the Taiwan Strait: the structure of a magma-poor rifted margin. Tectonics 35, 1782–1792.

Chen, S.-K., Wu, Y.-M., Hsu, Y.-J., Chan, Y.-C., 2017. Current crustal deformation of the Taiwan orogen reassessed by cGPS strain-rate estimation and focal mechanism stress inversion. Geophys. J. Int. 210, 228–239.

Cheng, C.-T., Chiou, S.-J., Lee, C.-T., Tsai, Y.-B., 2007. Study on probabilistic seismic hazard maps of Taiwan after Chi-Chi Earthquake. J. GeoEng. 2, 19–28.

Ching, K.-E., Rau, R.-J., Johnson, K.M., Lee, J.-C., Hu, J.-C., 2011. Present-day kinematics of active mountain building in Taiwan from GPS observations during 1995-2005. J. Geophys. Res. 116 https://doi.org/10.1029/2010JB008058.

Chiu, H.-T., 1975. Miocene stratigraphy and its relation to the Palaeogene rocks in west-Central Taiwan. Pet. Geol. Taiwan 12, 51–80.

Christensen, N.I., 1989. Pore pressure, seismic velocities, and crustal structure, in Geophysical framework of the continental United States, edited by L.C. Pakiser, and W.D. Mooney. Geol. Soc. Am. Mem. 172, 783–798.

Christensen, N.I., Stanley, D., 2003. Seismic velocities and densities of rocks. Int. Handb. Earthq. Eng. Seis. 81, 1587–1593.

Clark, M.B., Fisher, D.M., Lu, C.-Y., Chen, C.-H., 1993. Kinematic analyses of the Hsüehshan Range, Taiwan: a large-scale pop-up structure. Tectonics 12, 205–217.

Covey, M., 1986. The evolution of foreland basins to steady state: evidence from the western Taiwan foreland basin. In: Allen, P.A., Homewood, P. (Eds.), Foreland Basins, Spec. Pub. 8. Int. Ass. Sed. Blackwell, Oxford, UK, pp. 77–90.

Cukur, D., Horozal, S., Kim, D.C., Han, H.C., 2011. Seismic stratigraphy and structural analysis of the northern East China Sea Shelf Basin interpreted from multi-channel seismic reflection data and cross-section restoration. Mar. Pet. Geol. 28, 1003–1022.

Dahlen, F.A., Suppe, J., Davis, D., 1984. Mechanics of fold-and-thrust belts and accretionary wedges: cohesive Coulomg theory. J. Geophys. Res. 89, 10,087–10,101.

Dahlstrom, C.D.A., 1969. Balanced cross sections. Can. J. Earth Sci. 6, 743–757.

Davis, D., Suppe, J., Dahlen, F.A., 1983. Mechanics of fold-and-thrust belts and accretionary wedges. J. Geophys. Res. 88, 1153–1172.

De Paor, D.G., 1988. Balanced section in thrust belts part I: construction. Am. Assoc. Pet. Geol. Bull. 72, 73–90.

Deffontaines, B.O., Lacombe, O., Angelier, J., Chu, H.-T., Mouthereau, F., Lee, C.-T., Deramond, J., Lee, J.-F., Yu, M.-S., Liew, P.-M., 1997. Quaternary transfer faulting in the Taiwan Foorhills: evidence from a multisource approach. Tectonophysics 274, 61–82.

Deng, J.-M., Wang, T.-K., Yang, B.-J., Lee, C.-S., Liu, C.-S., Chen, S.-C., 2012. Crustal velocity structure off SW Taiwan in the northernmost South China Sea imaged from TAIGER OBS and MCS data. Mar. Geophys. Res. 33, 327–349.

Ding, W.-W., Li, J.-B., Li, M.-B., Qiu, X.-L., Fang, Y.-X., Tang, Y., 2008. A Cenozoic tectono-sedimentary model of the Tainan Basin, the South China Sea: evidence from multi-channel seismic profile. J. Zhejiang Univ. (Sci.) 9, 702–713.

Ernst, W.G., 1983. Mineral paragenesis in metamorphic rocks exposed along Tailuko Gorge, Central Mountain Range, Taiwan. J. Metamorph. Geol. 1, 305–329.

Hatcher, R.D., Williams, R.T., 1986. Mechanical model for single thrust sheets part I: taxonomy of crystalline thrust sheets and their relationship to the mechanical behaviour of orogenic belts. Geol. Soc. Am. Bull. 97, 975–985.

Hickman, J.B., Wiltschko, D.V., Hung, J.-H., Fang, P., Bock, Y., 2002. Structure and evolution of the active fold-and-thrust belt of southwestern Taiwan from Global Positioning System analysis. In: Bryne, T.B., Liu, C.-S. (Eds.), Geology and Geophysics of an Arc-Continent Collision, Taiwan, Geol. Soc. Am. Spec. Papers, vol. 358, pp. 75–92.

Ho, C.-S., 1988. An Introduction to the Geology of Taiwan: Explanatory Text of the Geological Map of Taiwan. Central Geol. Sur, Taipei, Taiwan.

Hong, E., 1997. Evolution of Pliocene to Pleistocene sedimentary environments in an arc-continent collision zone: evidence from the analyses of lithofacies and ichnofacies in the southwestern foothills of Taiwan. J. Asian Earth Sci. 15, 381–392.

Hossack, J.R., 1979. The use of balanced cross-sections in the calculation of orogenic contraction: a review. J. Geol. Soc. 136, 705–711.

Hsu, S.K., 2001. Subduction/collision complexities in the Taiwan–Ryukyu junction area: tectonics of the northwestern corner of the Philippine Sea plate. Terr. Atmos. Ocean. Sci. 209–230. Supplementary Issue.

Huang, S.T., Yang, K.-M., Hung, J.-H., Wu, J.C., Ting, H.H., Mei, W.W., Hsu, S.H., Lee, M., 2004. Deformation front development at the northeast margin of the Tainan basin, Tainan-Kaohsiung area, Taiwan. Mar. Geophys. Res. 25 (1–2), 139–156. https://doi.org/10.1007/s11001-005-0739-z.

Huang, C.-Y., Yen, Y., Zhao, Q.H., Lin, C.-T., 2012. Cenozoic stratigraphy of Taiwan: Window into rifting, stratigraphy and paleoceanography of South China Sea, Chinese Sc. Bull. 57, 3130–3149.

Huang, C.-Y., Chi, W.-R., Yan, Y., Yang, K.-M., Liew, P.-M., Wu, M.-S., Wu, J.-C., Zhang, C., 2013. The first record of Eocene tuff in a Paleogene rift basin near Nantou, Western Foothills, Central Taiwan. J. Asian Earth Sci. 69, 3–16.

Huang, H.-H., Wu, Y.-M., Song, X., Chang, C.-H., Kuo-Chen, H., Lee, S.-J., 2014a. Investigating the lithospheric velocity structures beneath the Taiwan region by nonlinear joint inversion of local and teleseismic P wave data: Slab continuity and deflection. Geophys. Res. Lett. 41, 6350–6357.
Huang, H.-H., Wu, Y.-M., Song, X., Chang, C.-H., Lee, S.-J., Chang, T.-M., Hsieh, H.-H., 2014b. Joint Vp and Vs tomography of Taiwan: Implications for subduction-collision orogeny. Earth Planet. Sci. Lett. 392, 177–191.
Huang, C.-Y., Shea, K.-H., Li, Q., 2017. A foraminiferal study on the Middle Eocene-Oligocene break-up unconformity in northern Taiwan and its correlation with IODP Site U1435 to constrain the onset event of South China Sea opening. J. Asian Earth Sci. 138, 439–465.
Hung, J.-H., Wiltschko, D., Lin, H.-C., Hickman, J.B., Fang, P., Bock, Y., 1999. Structure and motion of the Southwestern Taiwan fold and thrust belt. Terr. Atm. Ocean. Sci. 10 (3), 543–568.
Jahn, B.-M., Martineau, F., Peucat, J.J., Cornichet, J., 1986. Geochronology of the Tananao schist complex, Taiwan, and its regional tectonic significance. Tectonophysics 125, 103–124.
Jahn, B.-M., Chi, W.-R., Yui, T.-F., 1992. A late Permian formation of Taiwan marbles from Chia-Li well no.1: Pb-Pb isochron and Sr isotopic evidence, and its regional geological significance. J. Geol. Soc. China 35, 193–218.
Johnston, J.E., Christensen, N.I., 1992. Shear wave reflectivity, anisotropies, Poisson's ratios, and densities of a southern Appalachian Paleozoic sedimentary sequence. Tectonophysics 210, 1–20.
Johnston, J.E., Christensen, N.I., 1993. Compressional to shear velocity ratios in sedimentary rocks. Int. J. Rock Mech. Min. Sci. Geomech. Abs. 30, 751–754.
Judge, P.A., Allmendinger, R.W., 2011. Assessing uncertainties in balanced cross sections. J. Struct. Geol. 33, 458–467.
Kim, K.-H., Chiu, J.-M., Pujol, J., Chen, K.-C., Huang, B.-S., Yeh, Y.-H., Shen, P., 2005. Three-dimensional Vp and Vs structural models associated with the active subduction and collision tectonics in the Taiwan region. Geophys. J. Int. 162, 204–220.
Kley, J., Gangui, A.H., Krüger, D., 1996. Basement-involved blind thrusting in the eastern Cordillera oriental, southern Bolivia: evidence from cross-sectional balancing, gravimetric and magnetotelluric data. Tectonophyscis 259, 171–184.
Kuo-Chen, H., Wu, F.T., Roecker, S.W., 2012. Three-dimensional P velocity structures of the lithosphere beneath Taiwan from the analysis of TAIGER and related seismic data sets. J. Geophys. Res. 117 https://doi.org/10.1029/2011JB009108.
Kuo-Chen, H., Wu, F.T., Chang, W.-L., Chang, C.-Y., Cheng, C.-Y., Hirata, N., 2015. Is the Lishan fault of Taiwan active? Tectonophysics 661, 210–214.
Lacombe, O., Bellahsen, M., 2016. Thick-skinned tectonics and basement-involved fold–thrust belts: insights from selected Cenozoic orogens. Geol. Mag. 153, 763–810.
Lacombe, O., Mouthereau, F., 2002. Basement-involved shortening and deep detachment tectonics in forelands of orogens: insights from recent collision belts (Taiwan, Western Alps, Pyrenees). Tectonics 21, 12-11–12-22.
Lacombe, O., Mouthereau, F., Deffontaines, B., Anglier, J., Chu, H.-T., Lee, C.-T., 1999. Geometry and Quaternary kinematics of fold-and-thrust units of southwestern Taiwan. Tectonics 18, 1198–1223.
Lacombe, O., Mouthereau, F., Anglier, J., Chu, H.-T., Lee, J.-C., 2003. Frontal belt curvature and oblique ramp development at an obliquely collided irregular margin: Geometry and kinematics of NW Taiwan fold-thrust belt. Tectonics 22, 9-1–9-16.
Lan, C.-Y., Lee, C.-S., Yui, T.-F., Chu, H.-T., Jahn, B.-M., 2008. The tectono-thermal events of Taiwan and their relationaship with SE China. Terr. Atmos. Ocean. Sci. 19, 257–278.
Lee, T.-Y., Tang, C.-H., Ting, J.-S., Hsu, Y.-Y., 1993. Sequence stratigraphy of the Tainan Basin, offshore southwestern Taiwan. Pet. Geol. Taiwan 26, 119–158.
Lee, J.-C., Angelier, J., Chu, H.-T., 1997. Polyphase history and kinematics of a complex major fault zone in the northern Taiwan mountain belt: the Lishan Fault. Tectonophysics 274, 97–115.
Lester, R., Van Avendonk, H.J.A., McIntosh, K., Lavier, L., Liu, C.-S., Wang, T.-K., Wu, F., 2014. Rifting and magmatism in the northeastern South China Sea from wide-angle tomography and seismic reflection imaging. J. Geophys. Res. 119 https://doi.org/10.1002/2013JB010639.
Li, C.-F., Zhou, Z., Li, J., Hao, H., Geng, J., 2007. Structures of the northeasternmost South China Sea continental margin and ocean basin: geophysical constraints and tectonic implications. Mar. Geophys. Res. 28, 59–79.
Lin, A.T., Watts, A., 2002. Origin of the West Taiwan basin by orogenic loading and flexure of a rifted continental margin. J. Geophys. Res. 107 https://doi.org/10.1029/2001JB000669.
Lin, A., Watts, A., Hesselbo, P., 2003. Cenozoic stratigraphy and subsidence history of the South China Sea margin in the Taiwan region. Basin Res. 15, 453–478.
Lin, J.-Y., Sibuet, J.-C., Hsu, S.-K., 2005. Distribution of the East China Sea continental shelf basins and depths of magnetic sources. Earth Planet. Space 57, 1063–1072.
Lin, A.T., Liu, C.-S., Lin, C.C., Schnurle, P., Chen, G.-Y., Liao, W.-Z., Teng, L.-S., 2008. Tectonic features associated with the overriding of an accretionary wedge on top of a rifted continental margin: an example from Taiwan. Mar. Geol. 255, 186–203.
Lo, C.-H., Onstott, T.C., 1995. Rejuvenation of K–Ar systems for minerals in the Taiwan mountain belt. Earth Planet. Sci. Lett. 131, 71–98.
Loh, C.-H., Yeh, Y.-T., Jean, W.-Y., Yeh, Y.-H., 1991. Seismic hazard analysis in the Taiwan area using a bounded fault-rupture model. Bull. Seismol. Soc. Am. 81, 265–272.
Malavieille, J., Trullenque, G., 2009. Consequences of continental subduction on forearc basin and accretionary wedge deformation in SE Taiwan: insights from analogue modeling. Tectonophysics 466, 377–394.
Mavko, G., Mukerji, T., Dvorkin, J., 2009. The Rock Physics Handbook: Tools for Seismic Analysis in Porous Media. Cambridge University Press, Cambridge, U.K., 511 pp.
McIntosh, K., Van Avendonk, H., Lavier, L., Lester, W.R., Eakin, D., Wu, F., Liu, C.-S., Lee, C.-S., 2013. Inversion of a hyper-extended rifted margin in the southern Central Range of Taiwan. Geology 41, 871–874.
McIntosh, K., Lavier, L., Van Avendonk, H., Lester, R., Eakin, D., Liu, C.-S., 2014. Crustal structure and inferred rifting processes in the northeast South China Sea. Mar. Pet. Geol. 58, 612–626.
Mohn, G., Manatschal, G., Beltrando, M., Masini, E., Kusznir, N., 2012. Necking of the continental crust in magma-poor rifted margins: evidence from the fossil Alpine Tethys margins. Tectonics 31. https://doi.org/10.1029/2011TC002961.
Mouthereau, F., Lacombe, O., 2006. Inversion of the Paleogene Chinese continental margin and thick-skinned deformation in the Western Foreland of Taiwan. J. Struct. Geol. 28, 1977–1993.
Mouthereau, F., Petit, C., 2003. Rheology and strength of the Eurasian continental lithosphere in the foreland of the Taiwan collision belt: Constraints from seismicity, flexure, and structural styles. J. Geophys. Res. 108, 1-1–1-15.
Mouthereau, F., Lacombe, O., Deffontaines, B., Angelier, J., Chu, H.-T., Lee, C.-T., 1999. Quaternary transfer faulting and belt front deformation at Pakuashan (western Taiwan). Tectonics 18, 215–230.
Mouthereau, F., Lacombe, O., Deffontaines, B., Angelier, J., Brusset, S., 2001. Deformation history of the soutwestern Taiwan foreland thrust belt: insights from tectono-sedimentary analyses and balanced cross-sections. Tectonophysics 333, 293–322.
Mouthereau, F., Deffontaines, B., Lacombe, O., Angelier, J., 2002. Variations along the strike of the Taiwan thrust belt: basement control on structural style, wedge geometry, and kinematics, in Geology and Geophysics of an Arc-Continent Collision, Taiwan, edited by T.B. Byrne, and C.-S. Liu. Geol. Soc. Am. Spec. Pap. 358, 31–54.
Mouthereau, F., Lacombe, O., Meyer, B., 2006. The Zagros folded belt (Fars, Iran): constraints from topography and critical wedge modeling. Geophys. J. Int. 165, 336–356.
Mouthereau, F., Fillon, C., Ma, K.-F., 2009. Distribution of strain rates in the Taiwan orogenic wedge. Earth Planet. Sci. Lett. 284, 361–385.
Namson, J., 1981. Structure of the western foothills belt, Miaoli-Hsinchu area, Taiwan. 1. Southern part. Pet. Geol. Taiwan 18, 31–51.
Nissen, S.S., Hayes, D.E., Buhl, P., Diebold, J., 1995. Deep penetration seismic soundings across the northern margin of the South China Sea. J. Geophys. Res. 100, 22,407–22,433.
Pfiffner, O.A., 2017. Thick-skinned and thin-skinned tectonics: a global perspective. Preprints 2017, 2017070020.
Poblet, J., Lisle, R.J., 2011. Kinematic evolution and structural styles of fold-and-thrust belts. Geol. Soc. Lond. Spec. Publ. 349, 1–24.
Rodriguez-Roa, F.A., Wiltschko, D.V., 2010. Thrust belt architecture of the central and southern Western Foothills of Taiwan. In: Goffey, G.P., Craig, J., Needham, T., Scott, R. (Eds.), Hydrocarbons in Contractional Belts, Geol. Soc. London, Spec. Pub, vol. 348, pp. 137–168.
Shaw, C.-L., 1996. Stratigraphic correlation and isopach maps of the Western Taiwan Basin. Terr. Atmos. Ocean. Sci. 7, 333–360.
Shea, K.-S., Chang, H.-C., Huang, T.-Y., Ho, H.-C., Lin, W.-H., Lin, C.-W., Chen, H.-W., 2003. Geological Column in Taiwan. Central Geol. Surv, Taiwan, Taiwan.
Shi, X., Xu, H., Qiu, X., Xia, K., Yang, X., Li, Y., 2008. Numerical modeling on the relationship between thermal uplift and subsequent rapid subsidence: Discussion on the evolution of the Tainan Basin. Tectonics 27. https://doi.org/10.1029/2007TC002163.
Shyu, J.B.H., Sieh, K., Chen, Y.-G., Liu, C.-S., 2005. Neotectonic architecture of Taiwan and its implications for future large earthquakes. J. Geophys. Res. 110 https://doi.org/10.1029/2004JB003251.
Shyu, J.B.H., Chuang, Y.-R., Chen, Y.-L., Lee, Y.-R., Cheng, C.-T., 2016. A new on-land seismogenic structure source database from the Taiwan Earthquake Model (TEM) project for seismic hazard analysis of Taiwan. Terr. Atmos. Ocean. Sci. 27, 311–323.
Sibuet, J.C., Hsu, S.-K., 1997. Geodynamic of the Taiwan arc-continent collision. Tectonophysics 274, 221–252.
Sibuet, J.C., Hsu, S.-K., 2004. How was Taiwan created? Tectonophysics 379, 159–181.
Stanley, R.S., Hill, L.B., Chang, H.C., Hu, H.N., 1981. A transect through the metamorphic core of the central mountains, southern Taiwan. Mem. Geol. Soc. China 4, 443–473.
Suppe, J., 1980. A retrodeformable cross section of northern Taiwan. Proc. Geol. Soc. China 23, 46–55.
Suppe, J., 1981. Mechanics of mountain building and metamorphism in Taiwan. Geol. Soc. China Mem. 4, 67–89.
Suppe, J., 1986. Reactivated normal faults in the western Taiwan fold-and-thrust belt. Mem. Geol. Soc. China 7, 187–200.
Suppe, J., 1995. Present-day stress directions in western Taiwan inferred from borehole elongation. Pet. Geol. Taiwan 21, 1–12.
Suppe, J., Chang, Y.-L., 1983. Kink method applied to structural interpretation of seismic sections, Western Taiwan. Pet. Geol. Taiwan 19, 29–49.
Suppe, J., Namson, J., 1979. Fault-bend fold origin of frontal folds of the Western Taiwan fold-and-thrust belt. Pet. Geol. Taiwan 16, 1–18.
Tang, Q., Zheng, C., 2010. Seismic velocity structure and improved seismic image of the Southern Depression of the Tainan Basin from pre-stack depth migration. Terr. Atmos. Ocean. Sci. 21, 807–816.
Tavani, S., Granado, P., Corradetti, A., Camanni, G., Vignaroli, G., Manatschal, G., Mazzoli, S., Muñoz, J.A., Parente, M., 2021. Rift inheritance controls the switch from thin- to thick-skinned thrusting and basal décollement re-localization at the subduction-to-collision transition. Geol. Soc. Am. Bull. 133, 2157–2170.
Teng, L.-S., 1987. Stratigraphic records of the late Cenozoic Penglai Orogeny of Taiwan. Acta Geol. Taiwan. 25, 205–224.

Teng, L.-S., 1990. Geotectonic evolution of the late Cenozoic arc-continent collision in Taiwan. Tectonophysics 183, 57–76.
Teng, L.-S., 1992. Geotectonic evolution of Tertiary continental margin basins of Taiwan. Pet. Geol. Taiwan 27, 1–19.
Teng, L.-S., Lin, A.-T., 2004. Cenozoic tectonics of the China continental margin; Insights from Taiwan. In: Malpas, J., Fletcher, C.J.N., Ali, J.R., Aitchison, J.C. (Eds.), Aspects of the Tectonic Evolution of China, Geol. Soc. London, Spec. Pub, vol. 226, pp. 313–332.
Teng, L.S., Wang, Y., Tang, C.-H., Huang, C.-Y., Huang, T.-C., Yu, M.-S., Ke, A., 1991. Tectonic aspects of thePaleogene depositional basin of northern Taiwan. Proc. Geol. Soc. China 34, 313–336.
Tensi, J., Mouthereau, F., Lacombe, O., 2006. Lithospheric bulge in the West Taiwan Basin. Basin Res. 18, 277–299.
Thomas, W.A., 1990. Controls on locations of transverse zones in thrust belts. Eclogae Geol. Helv. 83, 727–744.
Tsai, C.-H., Hsu, S.-K., Yeh, Y.-C., Lee, C.-S., Xia, K., 2004. Crustal thinning of the northern continental margin of the South China Sea. Mar. Geophys. Res. 25, 63–78.
Waldhauser, F., 2001. hypoDD: a computer program to compute double-difference hypocenter locations. US Geol. Sur. Open File Rep. 01-113, 25 pp.
Waldhauser, F., Ellsworth, W.L., 2000. A double-difference earthquake location algorithm: Method and application to the northern Hayward Fault, California. Bull. Seismol. Soc. Am. 90, 1353–1368.
Wang, C.-Y., Li, C.-L., Su, F.-C., Leu, M.-T., Wu, M.-S., Lai, S.-H., Chern, C.-C., 2002. Structural mapping of the 1999 Chi-Chi earthquake fault, Taiwan, by seismic reflection methods. Terr. Atmos. Ocean. Sci. 13, 211–226.
Wang, J.-H., Hung, J.-H., Dong, J.-J., 2009. Seismic velocities, density, porosity, and permeability measured at a deep hole penetrating the Chelungpu fault in Central Taiwan. J. Asian Earth Sci. 36, 135–145.
Wiltschko, D.V., Hassler, L., Hung, J.-H., Liao, H.-S., 2010. From accretion to collision: Motion and evolution of the Chaochou Fault, southern Taiwan. Tectonics 29, 1–23.
Wintsch, R.P., Yang, H.-J., Li, X.-H., Tung, K.-A., 2011. Geochronologic evidence for a cold arc-continent collision: the Taiwan orogeny. Lithos 125, 236–248.
Wu, F.T., Rau, R.-J., Salzberg, D., 1997. Taiwan orogeny: thin-skinned or lithospheric collision? Teconophysics 274, 191–220.
Wu, Y.-M., Chang, C.-H., Zhao, L., Shyu, J.B.H., Chen, Y.-G., Sieh, K., Avouac, J.P., 2007. Seismic tomography of Taiwan: improved constraints from a dense network of strong motion stations. J. Geophys. Res. 112 https://doi.org/10.1029/2007JB004983.
Wu, Y.M., Chang, C.H., Zhao, L., Teng, T.L., Nakamura, M., 2008a. A comprehensive relocation of earthquakes in Taiwan from 1991 to 2005. Bull. Seismol. Soc. Am. 98, 1471–1481.
Wu, Y.-M., Zhao, L., Chang, C.-H., Hsu, Y.-J., 2008b. Focal-mechanism determination in Taiwan by genetic algorithm. Bull. Seismol. Soc. Am. 98, 651–661.
Wu, F.T., Kuo-Chen, H., McIntosh, K.D., 2014. Subsurface imaging, TAIGER experiments and tectonic models of Taiwan. J. Asian Earth Sci. 90, 173–208.
Wu, W.-N., Yen, Y.-T., Hsu, Y.-J., Wu, Y.-M., Lin, J.-Y., Hsu, S.-K., 2017. Spatial variation of seismogenic depths of crustal earthquakes in the Taiwan region: implications for seismic hazard assessment. Tectonophysics 708, 81–95.
Yang, K.-M., Ting, H.-H., Yuan, J., 1991. Structural stules and tectonic modes of Neogene extensional tectonics in southwestern Taiwan: implications for hydrocarbon exploration. Pet. Geol. Taiwan 26, 1–31.
Yang, K.-M., Huang, S.-T., Wu, J.-C., Ting, H.-H., Mei, W.-W., 2006. Review and new insights on foreland tectonics in western Taiwan. Int. Geol. Rev. 48, 910–941.
Yang, K.-M., Huang, S.-T., Wu, J.-C., Ting, H.-H., Mei, W.-W., Lee, M., Hsu, H.-H., Lee, C.-J., 2007. 3D geometry of the Chelungpu thrust system in Central Taiwan: its implications for active tectonics, Terr. Atmos. Ocean. Sci. 18, 143–181.
Yang, K.-M., Rau, R.-J., Chang, H.-Y., Hsieh, C.-Y., Ting, H.-H., Huang, S.-T., Wu, J.-C., Tang, Y.-J., 2016. The role of basement-involved normal faults in the recent tectonics of western Taiwan. Geol. Mag. 153, 1166–1191.
Yeh, Y.-H., Shih, R.-C., Lin, C.-H., Liu, C.-C., Yen, H.-Y., Huang, B.-S., Liu, C.-S., Chen, P.-Z., Huang, C.-S., Wu, C.-J., Wu, F.T., 1998. Onshore/offshore wide-angle deep seismic profiling in Taiwan. Terr. Atmos. Ocean. Sci. 9, 301–316.
Yeh, Y.-C., Hsu, S.-K., Doo, W.-B., Sibuet, J.-C., Liu, C.-S., Lee, C.-S., 2012. Crustal features of the northeastern South China Sea: insights from seismic and magnetic interpretations. Mar. Geophys. Res. 33, 307–326.
Yu, S.-B., Chen, H.Y., Kuo, L.C., 1997. Velocity field of GPS stations in the Taiwan area. Tectonophysics 274, 41–60.
Yue, L.-F., Suppe, J., Hung, J.-H., 2005. Structural geology of a classic thrust belt earthquake: the 1999 Chi-Chi earthquake Taiwan (Mw = 7.6). J. Struct. Geol. 27, 2058–2083.
Yui, T.-F., Okamoto, K., Usuki, T., Lan, C.-Y., Chu, H.-T., Liou, J.-G., 2009. Late Triassic–Late Cretaceous accretion/subduction in the Taiwan region along the eastern margin of South China: evidence from zircon SHRIMP dating. Int. Geol. Rev. 51, 304–328.
Yui, T.-F., Maki, K., Lan, C.-Y., Hirata, T., Chu, H.-T., Kon, Y., Yokoyama, T.D., Jahn, B.-M., Ernst, W.G., 2012. Detrital zircons from the Tananao metamorphic complex of Taiwan: implications for sediment provenance and Mesozoic tectonics. Tectonophysics 541–543, 31–42.
Zhao, M., Qiu, X., Xia, S., Xu, H., Wang, P., Wang, T.K., Lee, C.-S., Xia, K., 2010. Seismic structure in the northeastern South China Sea: S-wave velocity and Vp/Vs ratios derived from three-component OBS data. Tectonophysics 480, 183–197.
Zoback, M.L., 1992. First- and second-order patterns of stress in the lithosphere: the World stress map project. J. Geophys. Res. Earth 97, 11703–11728.